

Estimates for the Aerodynamic Coefficients of Ringsail and Disk-Gap-Band Parachutes Operating on Mars*

Juan R. Cruz¹ and Miranda L. Snyder²
NASA Langley Research Center, Hampton, Virginia, 23681

Models are presented for the aerodynamic coefficients of Supersonic Ringsail and Disk-Gap-Band parachutes as functions of total porosity, λ_T , Mach number, M , and total angle of attack, α_T (when necessary). The source aerodynamic coefficients data used for creating these models were obtained from a wind tunnel test of subscale parachutes. In this wind tunnel test, subscale parachutes of both parachute types were fabricated from two different fabrics with very different permeabilities. By varying the fabric permeability, while maintaining the parachute geometry constant, it was possible to vary λ_T . The fabric permeability test data necessary for the calculation of λ_T were obtained from samples of the same fabrics used to fabricate the subscale parachutes. Although the models for the aerodynamic coefficients are simple polynomial functions of λ_T and M , they are capable of producing good reproductions of the source data. The (λ_T, M) domains over which these models are applicable are clearly defined. The models are applicable to flight operations on Mars.

Nomenclature

a_0, a_1, a_2, a_3	= regressor coefficients for models of C_D and C_{Tot}
a_{12}, a_{13}, a_{23}	
$a_{0,\alpha_T}, a_{1,\alpha_T}, a_{2,\alpha_T}, a_{3,\alpha_T}$	= regressor coefficients for models of C_T, C_N , and $C_{m,SLCP}$ at a specific value of α_T
$a_{12,\alpha_T}, a_{13,\alpha_T}, a_{23,\alpha_T}$	
C	= stand-in symbol for C_D or C_{Tot}
C_{α_T}	= stand-in symbol for C_T, C_N , or $C_{m,SLCP}$ at a specific value of α_T
C_D	= drag coefficient (using S_0 as the reference area)
$C_{m,SLCP}$	= pitching moment coefficient about the suspension lines confluence point (using S_0 as the reference area and D_0 as the reference length)
C_N	= normal force coefficient (using S_0 as the reference area)
C_T	= tangential force coefficient (using S_0 as the reference area)
C_{Tot}	= total force coefficient (using S_0 as the reference area)
c_e	= effective porosity
D_F	= forebody maximum diameter
D_P	= projected diameter
D_0	= nominal diameter
K_1, K_2	= constants in the models for c_e
k	= discharge coefficient
L_{Riser}	= length of the riser
L_{SL}	= length of the suspension lines
M	= Mach number
M_{Eff}	= effective Mach number (wind tunnel test)
N_{SL}	= number of suspension lines

* An expanded version of this paper, including the source data, will be published as a NASA Technical Memorandum.

¹ Aerospace Engineer, Atmospheric Flight and Entry Systems Branch, AIAA Senior Member.

² Aerospace Engineer, Aeronautics Systems Engineering Branch.

R_{adj}^2	= adjusted coefficient of multiple determination
$\hat{R}e$	= unit Reynolds number
S_0	= nominal area
\mathbf{V}	= freestream airspeed vector
V_{Eff}	= effective airspeed
α_T	= total angle of attack
λ_g	= geometric porosity
λ_T	= total porosity
μ_{Eff}	= effective coefficient of viscosity
ρ_{Eff}	= effective density
DGB	= Disk-Gap-Band (parachute type)
EDL	= Entry, Descent, and Landing
JPL	= Jet Propulsion Laboratory
LaRC	= Langley Research Center
LowP	= “Low” Permeability fabric (PIA-C-43478D Type I)
MSL	= Mars Science Laboratory (mission)
PIA	= Parachute Industry Association
RMSE	= Root Mean Square Error
SIAD-R	= Supersonic Inflatable Aerodynamic Decelerator – Robotic
SLCP	= Suspension Lines Confluence Point
SSRS	= Supersonic Ringsail (parachute type)
StdP	= “Standard” Permeability fabric (PIA-C-7020D Type I)
TDT	= Transonic Dynamics Tunnel

I. Introduction

THE creation of flight dynamics simulations is often part of the design, development, and flight operations of missions that include entry, descent, and landing (EDL) in their concept of operation. Such flight dynamics simulations include models for many of the EDL sub-systems. For EDL systems that include a parachute, models of the parachute’s aerodynamic characteristics must be created for inclusion in the flight dynamics simulations. Examples of such parachute aerodynamic models, as created for the Mars Science Laboratory (MSL) mission, can be found in Reference 1. The parachute aerodynamic models for use in Mars-flight simulations need to take into account the unique operating conditions that missions encounter in the Martian atmosphere. Among these operating conditions are low atmospheric density, low dynamic pressure, and a broad range of Mach numbers (subsonic to supersonic).

This paper presents models for the aerodynamic coefficients of two parachute types suitable for use on Mars. The source data used to create these models were obtained from two test programs. The first test program involved wind tunnel testing of subscale parachutes; this test yielded the source aerodynamic coefficients data (Ref. 2). The second test program involved the measurement of the permeability characteristics of the fabrics used to fabricate the subscale parachute models used in the wind tunnel test (Ref. 3). Using these fabric permeability data, the total porosities, λ_T , of the parachutes were determined.

The drag, C_D , and total force, C_{Tot} , coefficients were modeled as functions of the total porosity, λ_T , and effective[†] Mach number, M_{Eff} . The static coefficients, C_T , C_N , and $C_{m,\text{SLCP}}$ (defined later in this paper), were modeled as functions of λ_T , M_{Eff} , and the total angle of attack, α_T . The range of applicability of the models are Mach numbers from approximately 0.25 to 0.50 (for all models) and total angles of attack less than or equal to 17 degrees (for the static coefficients models). The ranges of total porosity values for which the models are valid vary with the parachute type and are specified with the models in subsequent sections of this paper.

In the Source Tests and Data section of this paper the wind tunnel and fabric permeability tests are described, and the results relevant to the paper are presented. The following section, Drag and Total Force Coefficients Modeling,

[†] The term “effective” in this paper is used to describe the wind tunnel test operating conditions (e.g., Mach number, airspeed, density, coefficient of viscosity) at the parachute canopy, including the correction for wind tunnel blockage. In other words, the “effective” test conditions are the “freestream” test conditions corrected for wind tunnel blockage. In free-flight the effective and freestream conditions are identical.

describes the creation of, and resulting models for, C_D and C_{Tot} . Next, the Static Coefficients Modeling section similarly describes the creation of, and resulting models for, C_T , C_N , and $C_{m,SLCP}$. A Concluding Remarks section closes the main text of the paper.

II. Source Tests and Data

A. Wind Tunnel Test

A subsonic wind tunnel test of two parachute types for use on missions to Mars was conducted at the NASA Langley Research Center Transonic Dynamics Tunnel (TDT) during November 2014 using subscale model parachutes (Ref. 2). This test was conducted on two types of parachutes: Supersonic Ringsail (SSRS) and Disk-Gap-Band (DGB). These two parachute types, with their appropriate forebodies, are shown in Figures 1 and 2, respectively. The forebodies are the supersonic inflatable aerodynamic decelerator-robotic (SIAD-R) for the SSRS parachutes (Ref. 4), and the MSL backshell for the DGB parachutes (Ref. 1). The presence of the forebodies during the tests was important to capture the effect of their wakes on the parachute aerodynamic characteristics. The scales of the models were 5.0 percent (nominal) for the SSRS parachutes and 6.7 percent (nominal) for the DGB parachutes. All important elements of the parachute and forebody models were geometrically similar to their full-scale counterparts (e.g., trailing distance to parachute diameter ratio, forebody diameter to parachute diameter ratio). Details of the parachutes and forebodies are presented in Table 1. For each of the parachute types, models were fabricated using one of two fabrics described by the Parachute Industry Association (PIA) specifications PIA-C-7020D Type I or PIA-C-44378D Type I. For convenience in notation, these two fabric types will be denoted as “Standard” Permeability (StdP) and “Low” Permeability (LowP), respectively, for the rest of this paper. Thus, there were four parachute type/fabric combinations: SSRS/StdP, SSRS/LowP, DGB/StdP, and DGB/LowP. The two fabrics, StdP and LowP, were manufactured per the PIA specifications cited in References 5 and 6, respectively. These two parachute fabrics have very different permeability characteristics. Using two parachute fabrics with different permeability characteristics allowed for the total porosity of the parachutes to be varied while retaining the same parachute geometry and test conditions. Tests were conducted in air at a variety of densities[‡] and Mach numbers.

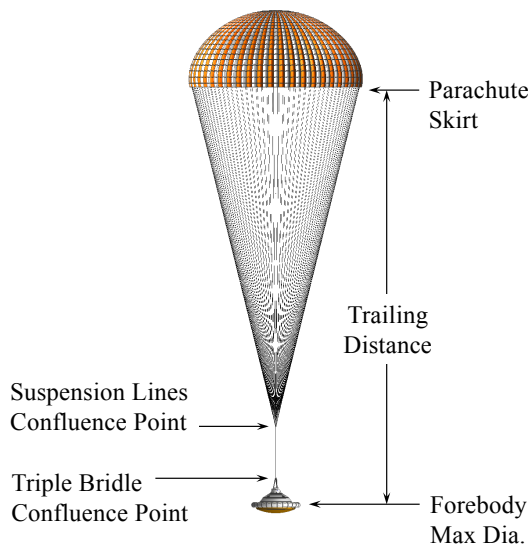


Figure 1. SSRS parachute and SIAD-R forebody overall geometry. (Image credit: JPL)

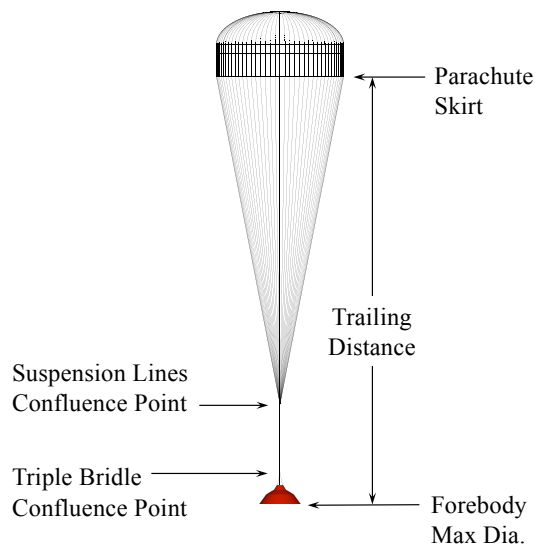


Figure 2. DGB parachute and MSL forebody (backshell) overall geometry. (Backshell image credit: Karl T. Edquist, NASA LaRC)

[‡] The TDT can operate at very low sub-atmospheric densities. For the wind tunnel test results presented herein, the density varied by a factor of 5.4.

Table 1. Details of the parachutes and forebodies.

	SSRS/SIAD-R		DGB/MSL Backshell	
	Full-Scale	Model	Full-Scale	Model
Scale (%)	100	5.0000	100	6.7041
Nominal Diameter, D_0 (ft)	100.1	5.003	70.04	4.696
Nominal Area, S_0 (ft ²)	7864	19.66	3853	17.32
Projected Diameter / Nominal Diameter, D_P/D_0		0.760		0.734
Geometric Porosity, λ_{g} (%)	14.9	15.0	12.80	12.85
Number of Suspension Lines, N_{SL}	96	48	80	40
Suspension Lines Length, L_{SL} (ft)	170.1	8.506	120.0	8.045
Riser Length, L_{Riser} (ft)	20.02	1.001	24.76	1.660
Forebody Maximum Diameter, D_F (ft)	19.69	0.984	14.54	0.975
Distance from Forebody Maximum Diameter to Triple Bridle Confluence Point (ft)	5.167	0.258	6.41	0.430

Notes to Table 1

- 1) All quantities are as-designed except for D_P/D_0 . The as-built parachute/forebody systems have slight variations from the numbers stated here.
- 2) The ratio D_P/D_0 was determined from photographs taken during the wind tunnel test. This is not an as-designed quantity.
- 3) The geometric porosity is calculated using the parachute's constrained vent area.
- 4) The riser length, L_{Riser} , is the distance from the suspension lines confluence point to the triple bridle confluence point. See Figures 1 and 2.
- 5) Additional details on the DGB parachute geometry can be found in Reference 1.

Results from this wind tunnel test included the parachute drag and total force coefficients (C_D and C_{Tot} , respectively) as well as the static coefficients (C_T , C_N , and $C_{m,SLCP}$). The forces on the forebodies were not measured; thus, all coefficients were for the parachutes, not the total parachute/forebody system. The test setup for the drag and total force coefficients is shown in Figure 3. The test setup for the static coefficients is shown in Figure 4. Definitions and sign conventions for the static coefficients are shown in Figure 5. Because the parachutes being considered here are assumed to be axisymmetric, the normal force associated with C_N lies in the total angle of attack plane.[§] Similarly, the pitching moment associated with $C_{m,SLCP}$ is perpendicular to the total angle of attack plane. Note that the moment defined by $C_{m,SLCP}$ is about the suspension lines confluence point (SLCP) as shown in Figure 5. The drag and total force coefficients test setup allowed the parachute to oscillate, rotating about the triple bridle confluence point (i.e., the attachment point to the wind tunnel balance). The drag and total force coefficients are “long-term” averages for time intervals during which the parachutes oscillated and occupied various locations downstream of the forebodies. The static coefficients are also “long-term” averages, but the parachute's total angle of attack was held at a fixed value by the test setup during the data acquisition time intervals. All coefficients used the parachute nominal area, S_0 , as the reference area. Moment coefficients used the parachute nominal diameter, D_0 , as the reference length.

This section has just included a brief summary of the model parachutes and wind tunnel test. For more details, the reader should consult Reference 2.

[§] The total angle of attack plane is defined as the plane that includes the freestream airspeed vector, \mathbf{V} , and the parachute's axis of symmetry. The plane of the paper in Figure 5 is the total angle of attack plane.

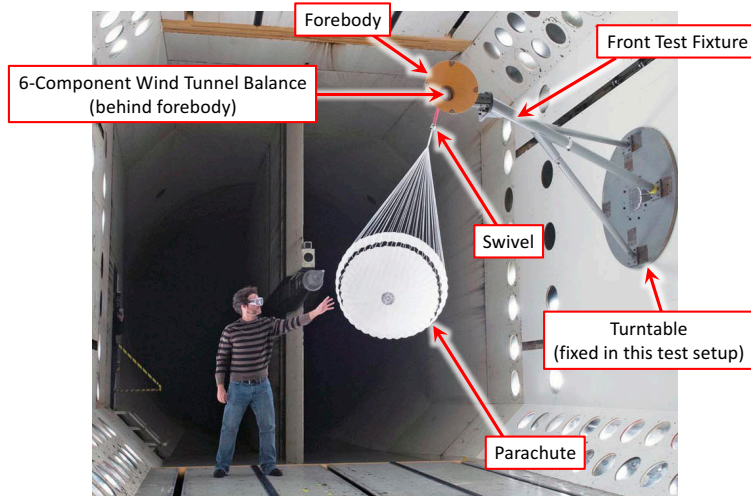


Figure 3. Drag and total force coefficients test setup.

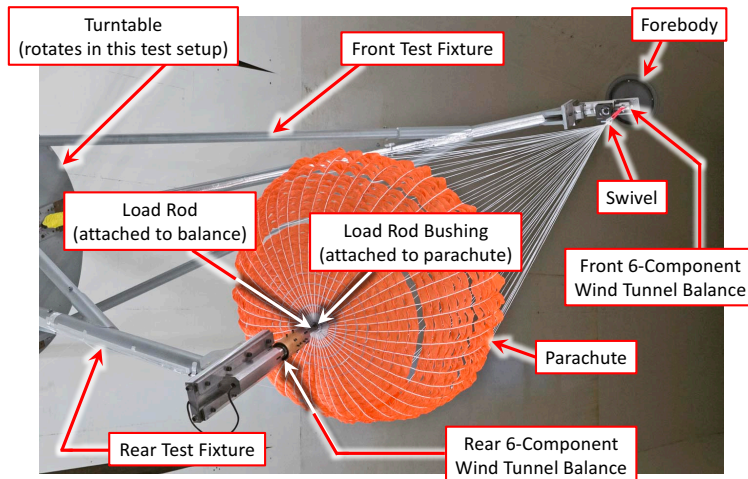


Figure 4. Static coefficients test setup.

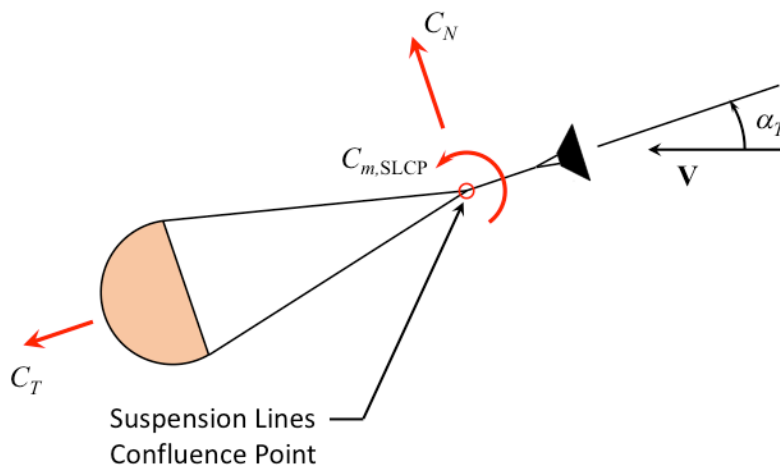


Figure 5. Definition of the static coefficients.

B. Fabric Permeability, Effective Porosity, and Total Porosity

The permeability[†] of the StdP and LowP fabrics was measured in air over a wide range of differential pressures. From these permeability results, the fabric's dimensionless effective porosities, c_e , were calculated and modeled as functions of the unit Reynolds number, $\hat{R}e$ (the dimension of $\hat{R}e$ is 1/Length). These models for $c_e(\hat{R}e)$ were of the form

$$c_e = \frac{-K_2}{2K_1\hat{R}e} + \sqrt{\left(\frac{K_2}{2K_1\hat{R}e}\right)^2 + \frac{1}{2K_1}} \quad (1)$$

where K_1 and K_2 are the effective porosity modeling constants (K_1 is dimensionless and K_2 has the dimension 1/Length), dependent on the fabric type. The value of $\hat{R}e$ was calculated for each parachute and test condition from

$$\hat{R}e = \frac{\rho_{\text{Eff}} V_{\text{Eff}}}{\mu_{\text{Eff}}} \left(\frac{D_0}{D_p} \sqrt{C_D} \right) \quad (2)$$

where D_p is the projected diameter of the parachute, and ρ_{Eff} , V_{Eff} , and μ_{Eff} are the effective test density, airspeed, and coefficient of viscosity, respectively, at the particular test condition (see footnote † for the definition of “effective”).

With c_e having been calculated, the total porosities of the parachutes were calculated from

$$\lambda_T = k\lambda_g + (1 - \lambda_g)c_e \quad (3)$$

where λ_g is the geometric porosity of the parachute, and k is the discharge coefficient. In the present work it was assumed that $k = 0.7$. The quantities k , λ_g , and λ_T are dimensionless.

The approach used here for modeling the fabric permeability and calculating the total porosity was presented by Lingard and Underwood in Reference 7 and Lingard in Reference 8. Details on the permeability and effective porosity of the StdP and LowP fabrics were presented in Reference 3.

C. Source Data

It was decided to model the drag, total force, and static coefficients using the total porosity and Mach number as the independent variables. These two quantities were chosen as the independent variables because they (1) are dimensionless, (2) are known to have significant effects on the aerodynamic characteristics, (3) are directly applicable to full-scale parachutes, and (4) yielded good models within the $(\lambda_T, M_{\text{Eff}})$ range of interest.

The source data used for modeling the drag and total force coefficients for the SSRS and DGB parachutes are presented in Tables 2 and 3, respectively. The Run/Group identification and values of λ_T and M_{Eff} for the static coefficients of the SSRS and DGB parachutes are presented in Tables 4 and 5, respectively. (Run/Group is a convenient identifier for a specific parachute type, fabric, and test condition.) The source data for the static coefficients C_T , C_N , and $C_{m,\text{SLCP}}$ as functions of α_T for the values of λ_T and M_{Eff} listed in Tables 4 and 5 can be found in Reference 9. The complete data set from the wind tunnel test in Reference 2 includes test conditions at lower values of M_{Eff} (0.09 to 0.17). These additional data were not considered in the present work for two reasons. First, because the lower Mach numbers are not likely to occur in a mission to Mars given Mars' thin atmosphere (for example, the descent Mach number of MSL at descent stage separation was 0.324, see Reference 10). Second, because trying to fit the simple models used in the present work over the complete data set (i.e., including the lower values of M_{Eff}) reduced the fidelity of the models in the range of Mach numbers of interest for Mars.

[†] Fabric permeability is the volumetric flow of fluid through the fabric per unit area per unit time (e.g., ft³/(ft²•s)) at a given differential pressure across the fabric.

Table 2. Drag and total force coefficient data for the SSRS parachutes.

Fabric Type	Run/Group	λ_r	M_{Eff}	C_D	C_{Tot}
StdP	15/47	0.1411	0.257	0.612	0.613
	15/46	0.1365	0.257	0.618	0.619
	15/45	0.1367	0.333	0.622	0.622
	15/44	0.1284	0.258	0.626	0.626
	15/43	0.1336	0.516	0.643	0.644
	15/42	0.1277	0.413	0.637	0.637
	15/41	0.1290	0.517	0.650	0.651
LowP	12/33	0.1063	0.261	0.658	0.658
	12/32	0.1062	0.337	0.667	0.668
	12/31	0.1060	0.263	0.651	0.655
	12/30	0.1060	0.420	0.676	0.677
	12/29	0.1061	0.523	0.702	0.702

Table 3. Drag and total force coefficient data for the DGB parachutes.

Fabric Type	Run/Group	λ_r	M_{Eff}	C_D	C_{Tot}
StdP	17/68	0.1212	0.255	0.564	0.564
	17/67	0.1163	0.254	0.565	0.565
	17/66	0.1166	0.331	0.568	0.568
	17/65	0.1083	0.255	0.573	0.573
	17/64	0.1134	0.513	0.586	0.586
	17/63	0.1073	0.409	0.583	0.584
	17/62	0.1087	0.512	0.589	0.589
LowP	16/56	0.0847	0.256	0.631	0.632
	16/55	0.0844	0.256	0.621	0.624
	16/54	0.0844	0.332	0.623	0.624
	16/53	0.0841	0.257	0.618	0.623
	16/52	0.0843	0.514	0.644	0.644
	16/51	0.0841	0.411	0.626	0.629
	16/60	0.0842	0.514	0.642	0.643

Table 4. Values of λ_T and M_{Eff} for the static coefficients data of the SSRS parachutes.

Fabric Type	Run/Group	λ_T	M_{Eff}
StdP	21/8	0.1411	0.257
	21/7	0.1365	0.257
	21/6	0.1368	0.333
	20/5	0.1292	0.257
	20/4	0.1340	0.515
	19/3	0.1275	0.410
	19/2	0.1295	0.514
LowP	25/29	0.1066	0.256
	25/28	0.1063	0.256
	25/27	0.1063	0.333
	25/26	0.1060	0.256
	25/25	0.1062	0.515
	25/24	0.1060	0.411
	25/23	0.1061	0.515

Table 5. Values of λ_T and M_{Eff} for the static coefficients data of the DGB parachutes.

Fabric Type	Run/Group	λ_T	M_{Eff}
StdP	31/43	0.1213	0.256
	29/41	0.1165	0.255
	29/40	0.1167	0.331
	29/39	0.1085	0.256
	29/38	0.1137	0.513
	29/37	0.1077	0.410
	29/36	0.1089	0.514
LowP	33/52	0.0847	0.256
	33/51	0.0844	0.257
	33/50	0.0844	0.333
	33/49	0.0841	0.258
	33/48	0.0843	0.515
	33/47	0.0841	0.412
	33/46	0.0842	0.515

II. Drag and Total Force Coefficients Modeling

Linear regression models of the general form

$$C = a_0 + a_1\lambda_T + a_2M_{\text{Eff}} + a_{12}\lambda_TM_{\text{Eff}} \quad (4)$$

were created for the SSRS and DGB parachutes using the method of least squares. The quantity C in Equation (4) represents either C_D or C_{Tot} as necessary. Not all regressor coefficients (i.e., a_0 , a_1 , a_2 , and a_{12}) were used for all models. The chosen models were those that maximized R_{adj}^2 subject to the requirement that all regressor coefficients had to have a p -value of 0.05 or less.[#] The linear regression models for C_D and C_{Tot} are presented in Table 6. Note that for these models to be valid, λ_T needs to be calculated as described by Equation (3) with $k = 0.7$.

[#] The regression and statistics were calculated using the JMP software published by SAS (Ref. 11).

Table 6. Models for C_D and C_{Tot} .

Parachute Type	Coef.	a_0	a_1	a_2	a_{12}	R^2_{adj}	RMSE	Max. p -value	Max. residual
SSRS	C_D	0.6031750	Not included	0.6312282	-4.199903	0.9808	0.00365	< 0.0001	0.006
	C_{Tot}	0.6052009	Not included	0.6339054	-4.245635	0.9798	0.00374	< 0.0001	0.006
DGB	C_D	0.7602148	-1.811319	0.0578995	Not included	0.9617	0.00579	0.0019	0.009
	C_{Tot}	0.7690143	-1.872619	0.0533234	Not included	0.9668	0.00552	0.0024	0.008

RMSE – Root Mean Square Error

The values of λ_T and M_{Eff} used to create the models (see Tables 2 and 3) are plotted versus each other in Figures 6 and 7 for the SSRS and DGB parachutes, respectively. Dotted lines show the boundaries of the convex hull domains defined by the (λ_T, M_{Eff}) points. Applying the models at points within the dotted lines is interpolation; otherwise it is extrapolation. Inequalities approximately defining the domain boundaries for the SSRS and DGB parachutes are presented in Equations (5) and (6), respectively. All inequalities must be satisfied for a point to be inside the domain. Using the models at points outside their convex hulls is not recommended as they may yield inaccurate values of the drag and total force coefficients.

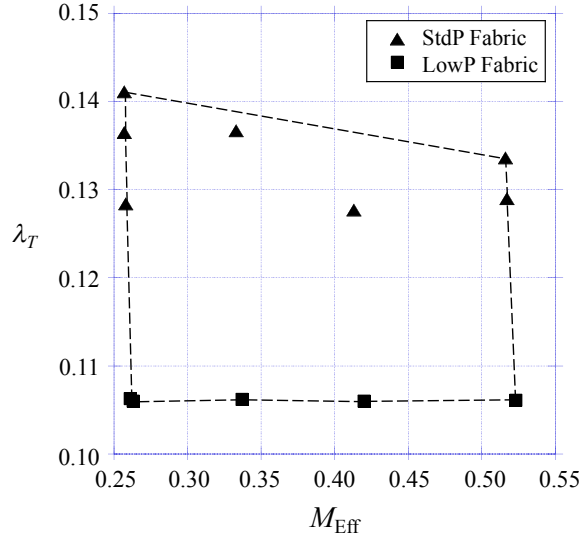


Figure 6. Domain of the C_D and C_{Tot} models for the SSRS parachutes.

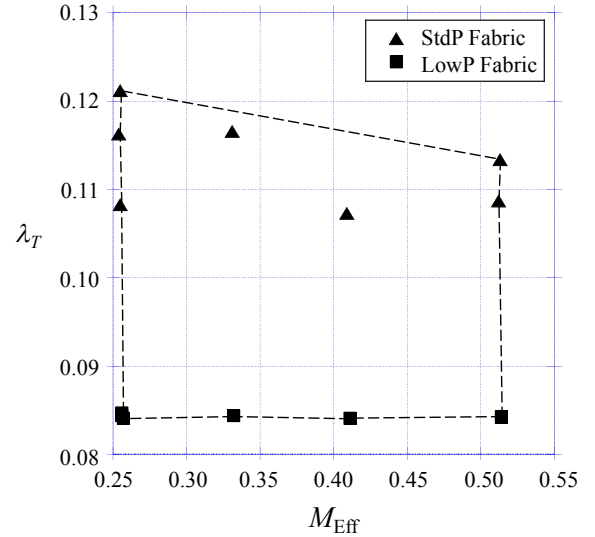


Figure 7. Domain of the C_D and C_{Tot} models for the DGB parachutes.

SSRS parachute domain definition for the C_D and C_{Tot} models

$$0.263 \leq M_{Eff} \leq 0.517 \quad (5a)$$

$$\lambda_T \geq 0.1063 \quad (5b)$$

$$\lambda_T \leq 0.1486 - 0.02906M_{Eff} \quad (5c)$$

DGB parachute domain definition for the C_D and C_{Tot} models

$$0.257 \leq M_{Eff} \leq 0.512 \quad (6a)$$

$$\lambda_T \geq 0.0847 \quad (6b)$$

$$\lambda_T \leq 0.1290 - 0.03057M_{Eff} \quad (6c)$$

Notice that the models defined by Equation (4) included only the linear and interaction regressors λ_T , M_{Eff} , and $\lambda_T M_{Eff}$. Quadratic regressors such as λ_T^2 and M_{Eff}^2 were intentionally not included in the models. The reason for this was that there were few data points inside the domains, as can be seen from Figures 6 and 7; most points

were on the boundaries of the domains. This limited number of data points within the domains casted doubt on the accurate identification of coefficients associated with quadratic regressors. In addition, models with quadratic coefficients would be more likely to yield inaccurate values of C_D and C_{Tot} if applied outside their domains (i.e., when extrapolating). The models defined by Equation (4) are considered to be more robust to minor extrapolations.

Other dimensionless independent variables and regressors were considered for inclusion in the linear regression models. Inclusion of other regressors yielded small improvements in the fidelity of the models as determined from R_{adj}^2 . However, these regressors exhibited significant collinearity. Thus, it was not possible to identify which regressor should be added to the models for full-scale parachute applications. Because of the small accuracy improvements, and the difficulty in identifying the appropriate additional regressor to add to the models, the models described by Equation (4) were used in the present work. Additional discussion on this topic is presented in Reference 9.

A partial check of the validity of the C_{Tot} model for the DGB parachute was conducted using data from the MSL mission (Ref. 10). Figure 8 shows the values of C_{Tot} for the MSL flight reconstruction and the present DGB model. The light gray line in this figure is the raw data from the MSL reconstruction over the Mach number interval for which the present DGB model is valid [see Equation (6)], and reconstruction data are available. This interval contains 89.92 s of the parachute phase of MSL; it ends with descent stage separation at a Mach number of 0.324. The oscillations in these raw data are expected; they are due to unsteadiness in the aerodynamic total force and parachute/payload oscillations. The dashed black line is a linear least squares fit to the raw data from the MSL reconstruction. (Note: the total uncertainty (includes both precision and bias uncertainties) in the MSL reconstruction on individual values of C_{Tot} was estimated to be ± 0.052 at the 95 percent level of confidence; see Reference 10, Table 7.) From the MSL reconstruction the values of λ_T and Mach number, M , were calculated.** (M is the equivalent of M_{Eff} in the present context.) The solid black line shows the results of the present DGB model using the values of λ_T and M obtained from the MSL reconstruction.†† The agreement between the linear fit of the reconstruction data and the present model is very good. At the lowest Mach number ($M = 0.324$), the two values of C_{Tot} agree within 0.5 percent. At the upper Mach number ($M = 0.512$), the two values of C_{Tot} agree within 5 percent. Given the many steps and data required to create the present model, the agreement with the MSL flight reconstruction data is encouraging with regard to the accuracy of the present model.

** The reconstructed values of C_{Tot} were used in lieu of C_D in Equation (2) to calculate $\hat{R}e$, and subsequently c_e and λ_T from Equations (1) and (3), respectively. The values of C_{Tot} and C_D were close enough to make this substitution acceptable. During the portion of the parachute phase discussed here ($0.324 \leq M \leq 0.512$), the total porosity was nearly constant, with a range of $0.0930 \leq \lambda_T \leq 0.0945$. This range in λ_T yields a variation of C_{Tot} less than 0.003.

†† Approximately 91 percent of the fabric used to fabricate the MSL parachute was PIA-C-7020B Type I and PIA-C-7020C Type I. These fabrics have the same permeability specifications as the PIA-C-7020D Type I (StdP) fabric. All three of these “7020” fabrics are woven using nylon fiber. The remaining 9 percent of the fabric used to fabricate the MSL parachute was woven to a proprietary Pioneer Aerospace specification using polyester fibers. (See Reference 10 for more details on the MSL parachute.) The polyester fabric had a measured fabric permeability 9 percent higher than the StdP fabric at a differential pressure of 0.5 inches of water (standard test conditions in the U.S.). In the analysis presented here, the MSL parachute is assumed to have been constructed in its entirety from StdP fabric. Because of the small area of the MSL parachute that used the polyester fabric, and the small difference in fabric permeability between the polyester fabric and the StdP fabric, the assumption that the entire MSL parachute was constructed from StdP fabric has a negligible effect on the values of C_{Tot} calculated by the model and reported here.

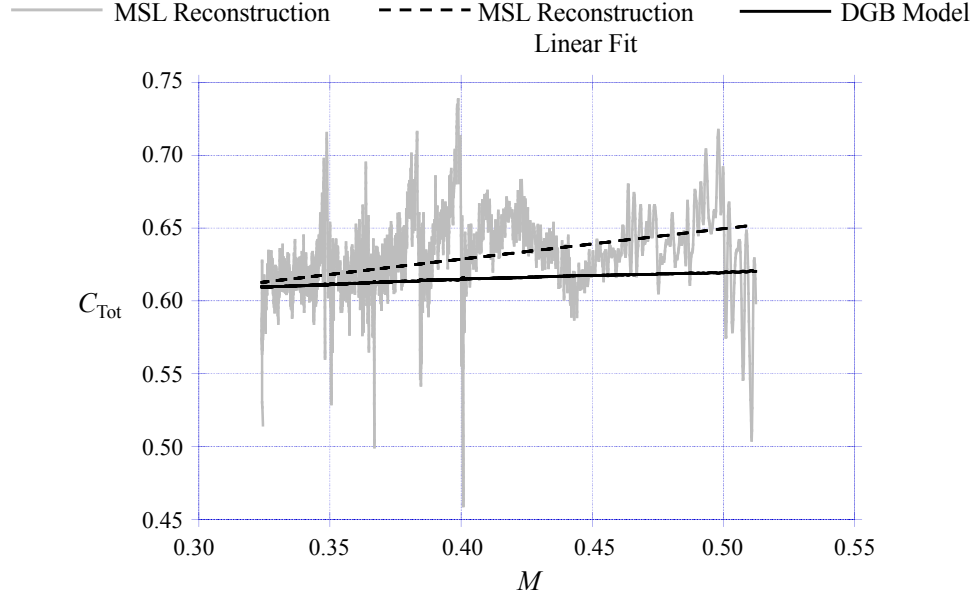


Figure 8. Comparison of the C_{Tot} values from the MSL reconstruction and the present model for the DGB parachute.

III. Static Coefficients Modeling

Linear regression models of the general form

$$C_{\alpha_T} = a_{0,\alpha_T} + a_{1,\alpha_T} \lambda_T + a_{2,\alpha_T} M_{\text{Eff}} + a_{12,\alpha_T} \lambda_T M_{\text{Eff}} \quad (7)$$

were created for the SSRS and DGB parachutes using the method of least squares.^{§§} The quantity C_{α_T} in Equation (7) represents C_T , C_N , or $C_{m,\text{SLCP}}$ as necessary for a specific value of α_T . The regressor coefficients, a_{0,α_T} , a_{1,α_T} , a_{2,α_T} , and a_{12,α_T} , are associated with the same specific value of α_T associated with its corresponding C_{α_T} . Thus, as an example, for a given parachute type (SSRS or DGB) at $\alpha_T = 4.8^\circ$,

$$C_{T,\alpha_T=4.8^\circ} = a_{0,\alpha_T=4.8^\circ} + a_{1,\alpha_T=4.8^\circ} \lambda_T + a_{2,\alpha_T=4.8^\circ} M_{\text{Eff}} + a_{12,\alpha_T=4.8^\circ} \lambda_T M_{\text{Eff}} \quad (8)$$

where the values of the regressor coefficients, $a_{0,\alpha_T=4.8^\circ}$, $a_{1,\alpha_T=4.8^\circ}$, $a_{2,\alpha_T=4.8^\circ}$, and $a_{12,\alpha_T=4.8^\circ}$, are specific to C_T at $\alpha_T = 4.8^\circ$ and the parachute type. All models retained all regressor coefficients, a_{0,α_T} , a_{1,α_T} , a_{2,α_T} , and a_{12,α_T} .^{¶¶} The linear regression models for C_T , C_N , and $C_{m,\text{SLCP}}$ (i.e., the values of the regressor coefficients, a_{0,α_T} , a_{1,α_T} , a_{2,α_T} , and a_{12,α_T}) are presented in the Appendix. For the static coefficient models to be valid, λ_T needs to be calculated as described by Equation (3) with $k = 0.7$.

The values of λ_T and M_{Eff} used to create the models (see Tables 4 and 5) are plotted versus each other in Figures 9 and 10 for the SSRS and DGB parachutes, respectively. Dotted lines show the boundaries of the convex hull domains defined by the $(\lambda_T, M_{\text{Eff}})$ points. Applying the models at points within the dotted lines is interpolation; otherwise it is extrapolation. Inequalities approximately defining the domain boundaries for the SSRS and DGB parachutes are presented in Equations (9) and (10), respectively. These inequalities must be satisfied for a point to be inside the domains. As with the C_D and C_{Tot} models, using the static coefficient models at points outside their convex hulls is not recommended as they may yield inaccurate values of the static coefficients.

^{§§} The source static coefficient source data (i.e., C_T , C_N , and $C_{m,\text{SLCP}}$ as functions of α_T), are presented in Reference 9 for the Run/Group and values of λ_T and M_{Eff} specified in Tables 4 and 5. The range of α_T for these data are from 0 to 17 degrees, at intervals of 0.2 degrees. These source static coefficient data were used to create the models.

^{¶¶} Note that functions of α_T were not used in the models for the static coefficients. The relationships between the static coefficients and α_T are complex and difficult to model with simple functions.

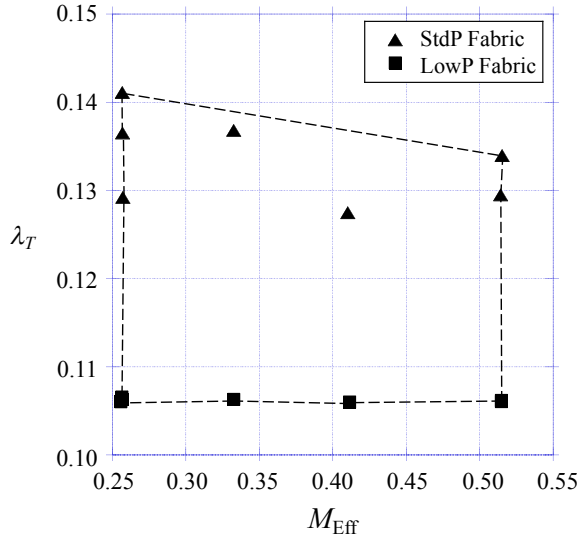


Figure 9. Domain of the C_T , C_N , and $C_{m,SLCP}$ models for the SSRS parachutes.

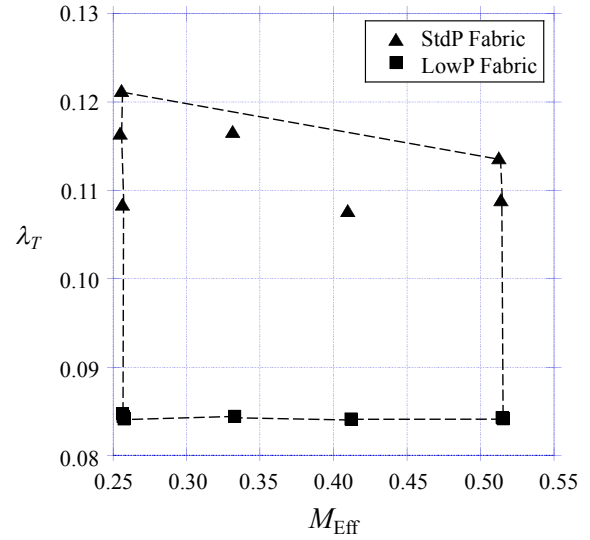


Figure 10. Domain of the C_T , C_N , and $C_{m,SLCP}$ models for the DGB parachutes.

SSRS parachute domain definition for the static coefficient models

$$0.257 \leq M_{\text{Eff}} \leq 0.514 \quad (9a)$$

$$\lambda_T \geq 0.1066 \quad (9b)$$

$$\lambda_T \leq 0.1482 - 0.02765M_{\text{Eff}} \quad (9c)$$

DGB parachute domain definition for the static coefficient models

$$0.257 \leq M_{\text{Eff}} \leq 0.513 \quad (10a)$$

$$\lambda_T \geq 0.0847 \quad (10b)$$

$$\lambda_T \leq 0.1289 - 0.02964M_{\text{Eff}} \quad (10c)$$

The models defined by Equation (7) include only the linear and interaction regressors: λ_T , M_{Eff} , and $\lambda_T M_{\text{Eff}}$. Quadratic regressors such as λ_T^2 and M_{Eff}^2 were intentionally not included in the models. The reasons for this selection of regressors are the same as those described for the drag and total force coefficient models.

Other dimensionless independent variables and regressors were considered for inclusion in the linear regression models for the static coefficients. As was the case with the C_D and C_{Tot} models, adding other dimensionless regressors yielded some improvements in the fidelity of the static coefficient models. However, it was decided not to include any additional regressors to the models—the improvements were considered to have detrimental effects on the applicability of the models to full-scale parachutes. Thus, the models described by Equation (7) were used in the present work. Additional discussion on this topic is presented in Reference 9.

The fidelity of the models was evaluated by comparing the source static coefficient data against the values predicted by the models. The following observations were made from these comparisons:

- 1) In general the models performed well in reproducing the source static coefficient data.
- 2) The models were better at reproducing the source data for C_T as compared to C_N and $C_{m,SLCP}$.
- 3) The overall fidelity of the models was better for parachutes fabricated from LowP fabric as compared to those fabricated from StdP fabric.
- 4) No significant difference was found in the overall fidelity of the models for the SSRS parachutes and the DGB parachutes.

Some of the Run/Group with the largest discrepancies between the source static coefficient data and the models were selected for more detailed inspection, including consideration of the uncertainties associated with the source static coefficient data. The largest difference in C_T between the source static coefficient data and the model was

observed in Run 19, Group 3 (SSRS/StdP parachute, $\lambda_T = 0.1275$, $M_{\text{Eff}} = 0.410$). Figure 11 shows C_T versus α_T for the source data (thin solid line with uncertainty bars) and the model (dashed line). The uncertainty bars in Figure 11 show the 95 percentile confidence interval around the source data, including both precision and bias uncertainty. As can be seen from Figure 11, the model values are within the specified confidence interval around the source data. Thus, the difference between the source data and the model values vis-à-vis the confidence interval, and the absolute maximum difference between the source data and the model values (1.9 percent), do not constitute a significant degradation in the accuracy of the values of C_T calculated from the model. For all other Runs/Groups the difference between the source data and model values for C_T are less than that for Run 19, Group 3.

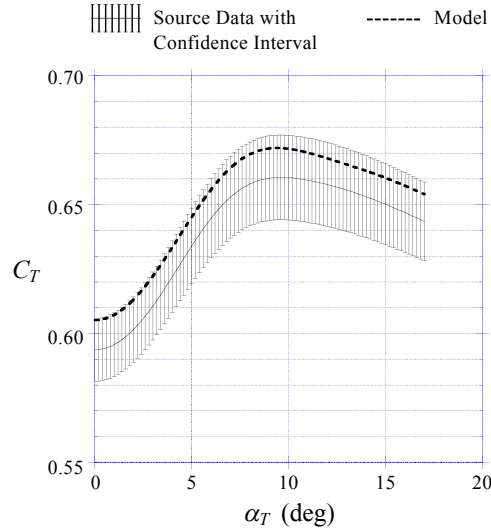


Figure 11. Static coefficient C_T versus α_T for the SSRS/StdP parachute, Run 19/Group 3, $\lambda_T = 0.1275$, $M_{\text{Eff}} = 0.410$.

Significant differences in C_N and $C_{m,\text{SLCP}}$ were observed for Run 20, Group 5 (SSRS/StdP parachute, $\lambda_T = 0.1292$, $M_{\text{Eff}} = 0.257$) and Run 25, Group 28 (SSRS/LowP parachute, $\lambda_T = 0.1063$, $M_{\text{Eff}} = 0.256$). Figure 12 shows C_N and $C_{m,\text{SLCP}}$ versus α_T for the source data (thin solid lines with uncertainty bars) and the models (dashed lines) for Run/Group 20/5 and 25/28. The meaning of the uncertainty bars is the same as that for Figure 11. For the Runs/Groups shown in Figure 12, the models yield C_N and $C_{m,\text{SLCP}}$ values outside the confidence intervals for their respective source data for some values of α_T .

The differences between the source static coefficients data and the models have multiple sources, two of which are discussed here. First is the simplicity of the model in Equation (7), which contains only the first order linear terms in l_T and M_{Eff} and their interaction term $\lambda_T M_{\text{Eff}}$. Even if the only independent variables retained were λ_T and M_{Eff} , more complex models (e.g., models including quadratic terms and/or transformations of λ_T and M_{Eff}) are likely to have yielded better fidelity vis-à-vis the source static coefficients data. However, as discussed earlier, the simpler models used herein were chosen due to the distribution of the source static coefficients data within their domains and the perceived higher robustness of simpler models with respect to minor extrapolations in their use. A second source for the differences between the source static coefficients data and the models is likely to be the absence of other relevant dimensionless coefficients as independent variables (this issue is discussed in Reference 9).

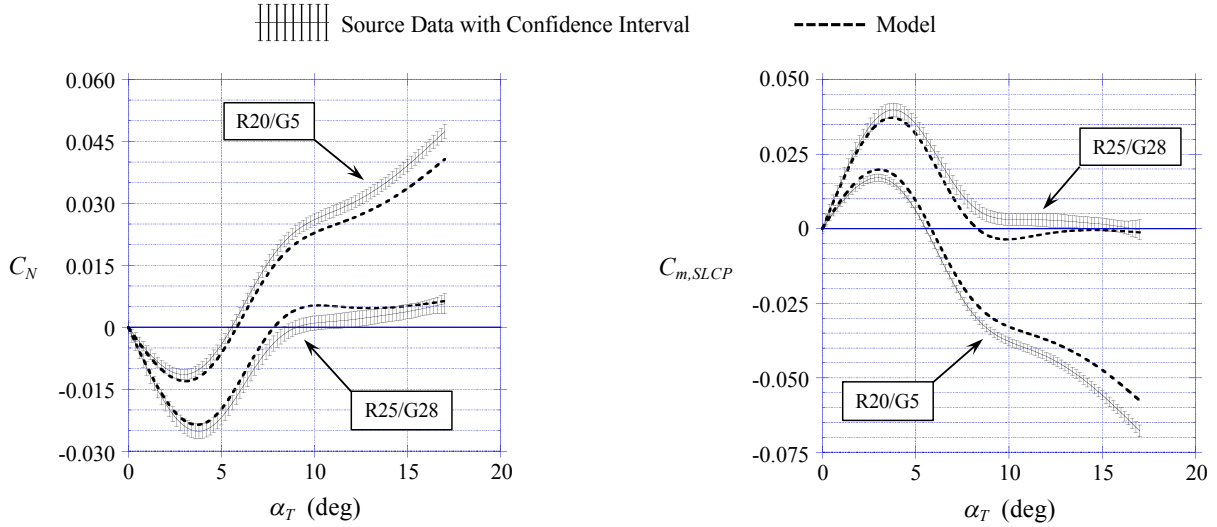


Figure 13. Static coefficients C_N and $C_{m,SLCP}$ versus α_T for the SSRS/StdP parachute, Run 20/Group 5, $\lambda_T = 0.1292$, $M_{Eff} = 0.257$, and the SSRS/LowP parachute, Run 25/Group 28, $\lambda_T = 0.1063$, $M_{Eff} = 0.256$.

The models were used to calculate the static coefficients of the MSL parachute, assuming it was fabricated from StdP fabric (see footnote ††). These calculations were performed at two flight conditions: the upper and lower Mach number limits shown in Figure 8. The corresponding values of λ_T were calculated from the reconstructed MSL flight parameters (e.g., airspeed, density, coefficient of viscosity) at the two Mach numbers. The values of λ_T and M were (0.0944, 0.324) and (0.0939, 0.512). These combinations of λ_T and M were within the domain of the models specified in Equation (10) for the DGB parachutes. The static coefficients thus calculated are shown in Figure 13. The differences between the two flight conditions are principally due to the Mach number. Because the total porosity is nearly the same for these two flight conditions, total porosity is not the primary source of the differences between the curves in Figure 13. Reconstructed values of the static coefficients for the MSL descent on Mars are not available; there was insufficient data to reconstruct the static coefficients. Thus, a validation comparison cannot be conducted for the modeled static coefficients shown in Figure 13.

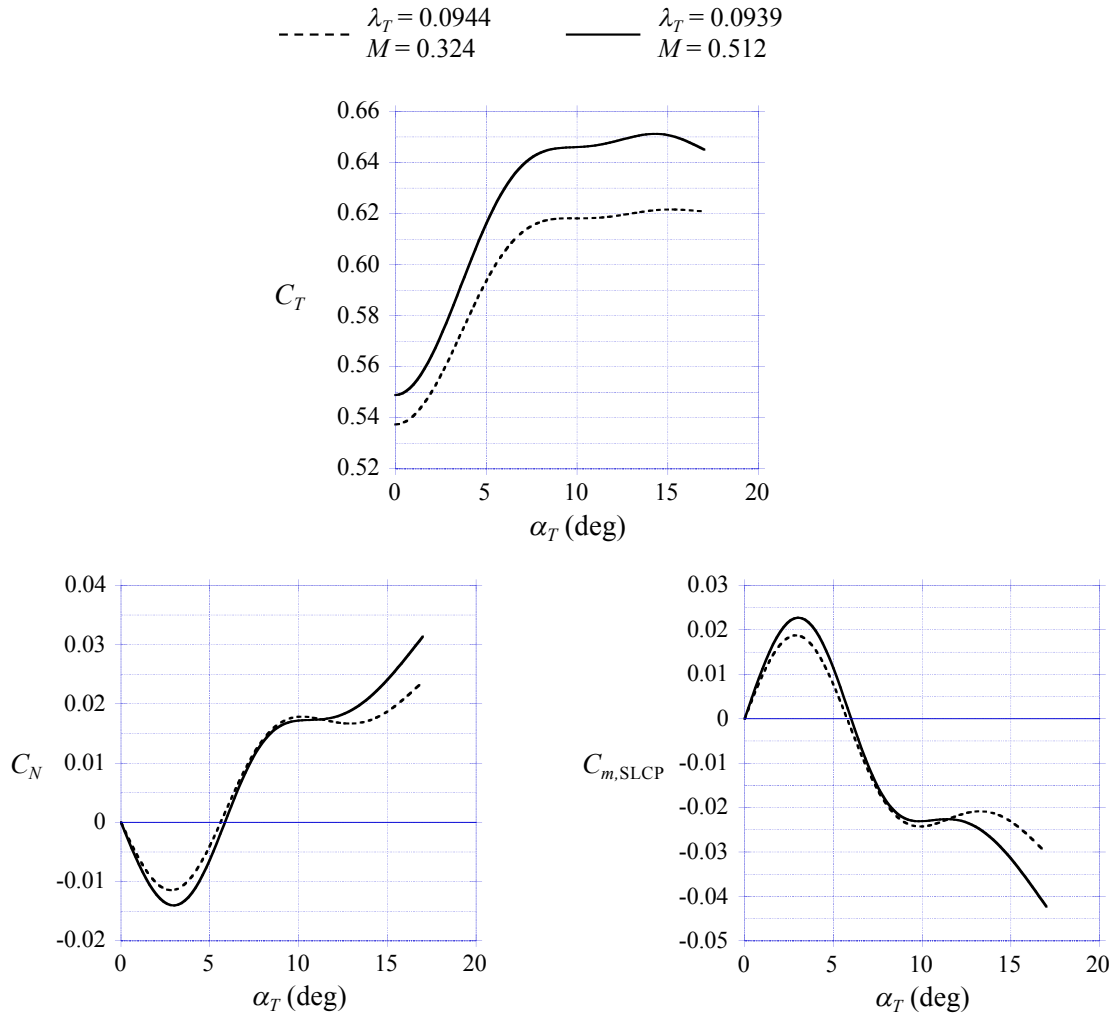


Figure 14. Modeled static coefficients for MSL during terminal descent.

IV. Concluding Remarks

Models were presented for the aerodynamic coefficients (i.e., C_D , C_{Tot} , C_T , C_N , and $C_{m,SLCP}$) of SSRS and DGB parachutes as functions of total porosity, λ_T , Mach number, M , and total angle of attack, α_T (when necessary). The source aerodynamic coefficients data for creating these models were obtained during the wind tunnel test described in Reference 2. The total porosity for these parachutes was calculated using the fabric permeability test data presented in Reference 3. Although the models are simple functions of λ_T and M , they provide good reproductions of the source aerodynamic coefficient data. The (λ_T, M) domains of applicability for these models were defined. These domains are applicable to flight operations on Mars.

The models presented herein are not unique—other models could be created from the source data. To make this possible the aerodynamic coefficients source data are presented in Tables 2 and 3 (drag and total force coefficients) and Reference 9 (static coefficients).

APPENDIX: MODELS FOR THE STATIC COEFFICIENTS

Table A1. Model for C_T - SSRS parachute.

α_T (deg)	a_{0,α_T}	a_{1,α_T}	a_{2,α_T}	a_{12,α_T}
0.0	7.95735E-01	-1.66648E+00	1.33957E-01	-6.30962E-01
0.2	7.95753E-01	-1.66624E+00	1.34475E-01	-6.34325E-01
0.4	7.95804E-01	-1.66551E+00	1.36025E-01	-6.44387E-01
0.6	7.95890E-01	-1.66432E+00	1.38593E-01	-6.61059E-01
0.8	7.96010E-01	-1.66268E+00	1.42165E-01	-6.84244E-01
1.0	7.96165E-01	-1.66062E+00	1.46726E-01	-7.13841E-01
1.2	7.96360E-01	-1.65819E+00	1.52248E-01	-7.49648E-01
1.4	7.96595E-01	-1.65543E+00	1.58696E-01	-7.91418E-01
1.6	7.96871E-01	-1.65235E+00	1.66037E-01	-8.38941E-01
1.8	7.97185E-01	-1.64897E+00	1.74239E-01	-8.92009E-01
2.0	7.97539E-01	-1.64532E+00	1.83270E-01	-9.50413E-01
2.2	7.97927E-01	-1.64139E+00	1.93100E-01	-1.01397E+00
2.4	7.98346E-01	-1.63717E+00	2.03673E-01	-1.08232E+00
2.6	7.98795E-01	-1.63271E+00	2.14915E-01	-1.15497E+00
2.8	7.99277E-01	-1.62805E+00	2.26748E-01	-1.23137E+00
3.0	7.99792E-01	-1.62324E+00	2.39093E-01	-1.31100E+00
3.2	8.00341E-01	-1.61832E+00	2.51871E-01	-1.39331E+00
3.4	8.00923E-01	-1.61333E+00	2.64978E-01	-1.47761E+00
3.6	8.01540E-01	-1.60834E+00	2.78296E-01	-1.56307E+00
3.8	8.02194E-01	-1.60341E+00	2.91703E-01	-1.64885E+00
4.0	8.02887E-01	-1.59860E+00	3.05081E-01	-1.73414E+00
4.2	8.03619E-01	-1.59399E+00	3.18311E-01	-1.81811E+00
4.4	8.04389E-01	-1.58960E+00	3.31274E-01	-1.89996E+00
4.6	8.05194E-01	-1.58547E+00	3.43852E-01	-1.97888E+00
4.8	8.06029E-01	-1.58162E+00	3.55926E-01	-2.05408E+00
5.0	8.06893E-01	-1.57809E+00	3.67379E-01	-2.12474E+00
5.2	8.07780E-01	-1.57490E+00	3.78106E-01	-2.19018E+00
5.4	8.08683E-01	-1.57204E+00	3.88056E-01	-2.25005E+00
5.6	8.09591E-01	-1.56951E+00	3.97194E-01	-2.30413E+00
5.8	8.10495E-01	-1.56728E+00	4.05482E-01	-2.35221E+00
6.0	8.11387E-01	-1.56533E+00	4.12885E-01	-2.39407E+00
6.2	8.12258E-01	-1.56367E+00	4.19371E-01	-2.42953E+00
6.4	8.13100E-01	-1.56226E+00	4.24951E-01	-2.45868E+00
6.6	8.13902E-01	-1.56107E+00	4.29658E-01	-2.48180E+00
6.8	8.14652E-01	-1.56003E+00	4.33521E-01	-2.49912E+00
7.0	8.15337E-01	-1.55911E+00	4.36571E-01	-2.51092E+00
7.2	8.15949E-01	-1.55825E+00	4.38845E-01	-2.51746E+00
7.4	8.16480E-01	-1.55743E+00	4.40408E-01	-2.51923E+00
7.6	8.16923E-01	-1.55659E+00	4.41339E-01	-2.51683E+00
7.8	8.17267E-01	-1.55568E+00	4.41720E-01	-2.51085E+00
8.0	8.17505E-01	-1.55463E+00	4.41632E-01	-2.50189E+00
8.2	8.17627E-01	-1.55338E+00	4.41163E-01	-2.49061E+00
8.4	8.17629E-01	-1.55188E+00	4.40411E-01	-2.47772E+00
8.6	8.17509E-01	-1.55009E+00	4.39467E-01	-2.46390E+00
8.8	8.17265E-01	-1.54796E+00	4.38426E-01	-2.44983E+00

Continued

Table A1. Concluded.

α_T (deg)	a_{0,α_T}	a_{1,α_T}	a_{2,α_T}	a_{12,α_T}
9.0	8.16894E-01	-1.54545E+00	4.37380E-01	-2.43621E+00
9.2	8.16395E-01	-1.54252E+00	4.36418E-01	-2.42366E+00
9.4	8.15776E-01	-1.53919E+00	4.35603E-01	-2.41266E+00
9.6	8.15044E-01	-1.53547E+00	4.34992E-01	-2.40359E+00
9.8	8.14207E-01	-1.53137E+00	4.34644E-01	-2.39686E+00
10.0	8.13273E-01	-1.52691E+00	4.34614E-01	-2.39290E+00
10.2	8.12251E-01	-1.52211E+00	4.34949E-01	-2.39201E+00
10.4	8.11157E-01	-1.51704E+00	4.35636E-01	-2.39409E+00
10.6	8.10011E-01	-1.51182E+00	4.36646E-01	-2.39891E+00
10.8	8.08831E-01	-1.50653E+00	4.37950E-01	-2.40624E+00
11.0	8.07638E-01	-1.50128E+00	4.39518E-01	-2.41585E+00
11.2	8.06448E-01	-1.49615E+00	4.41321E-01	-2.42751E+00
11.4	8.05278E-01	-1.49124E+00	4.43322E-01	-2.44094E+00
11.6	8.04143E-01	-1.48663E+00	4.45478E-01	-2.45582E+00
11.8	8.03060E-01	-1.48243E+00	4.47745E-01	-2.47182E+00
12.0	8.02044E-01	-1.47871E+00	4.50080E-01	-2.48861E+00
12.2	8.01112E-01	-1.47558E+00	4.52439E-01	-2.50587E+00
12.4	8.00272E-01	-1.47308E+00	4.54794E-01	-2.52337E+00
12.6	7.99533E-01	-1.47129E+00	4.57115E-01	-2.54091E+00
12.8	7.98904E-01	-1.47027E+00	4.59373E-01	-2.55825E+00
13.0	7.98394E-01	-1.47009E+00	4.61539E-01	-2.57516E+00
13.2	7.98011E-01	-1.47081E+00	4.63588E-01	-2.59143E+00
13.4	7.97754E-01	-1.47244E+00	4.65515E-01	-2.60703E+00
13.6	7.97622E-01	-1.47498E+00	4.67324E-01	-2.62197E+00
13.8	7.97613E-01	-1.47843E+00	4.69014E-01	-2.63624E+00
14.0	7.97725E-01	-1.48279E+00	4.70588E-01	-2.64985E+00
14.2	7.97955E-01	-1.48807E+00	4.72051E-01	-2.66282E+00
14.4	7.98298E-01	-1.49421E+00	4.73414E-01	-2.67523E+00
14.6	7.98744E-01	-1.50118E+00	4.74697E-01	-2.68720E+00
14.8	7.99287E-01	-1.50894E+00	4.75915E-01	-2.69883E+00
15.0	7.99917E-01	-1.51742E+00	4.77084E-01	-2.71024E+00
15.2	8.00627E-01	-1.52660E+00	4.78221E-01	-2.72153E+00
15.4	8.01410E-01	-1.53641E+00	4.79334E-01	-2.73273E+00
15.6	8.02256E-01	-1.54678E+00	4.80430E-01	-2.74388E+00
15.8	8.03154E-01	-1.55763E+00	4.81517E-01	-2.75503E+00
16.0	8.04096E-01	-1.56887E+00	4.82602E-01	-2.76623E+00
16.2	8.05071E-01	-1.58043E+00	4.83694E-01	-2.77751E+00
16.4	8.06073E-01	-1.59224E+00	4.84792E-01	-2.78888E+00
16.6	8.07096E-01	-1.60424E+00	4.85895E-01	-2.80031E+00
16.8	8.08132E-01	-1.61638E+00	4.87002E-01	-2.81178E+00
17.0	8.09176E-01	-1.62859E+00	4.88111E-01	-2.82328E+00

Table A2. Model for C_N - SSRS parachute.

α_T (deg)	a_{0,α_T}	a_{1,α_T}	a_{2,α_T}	a_{12,α_T}
0.0	0.00000E+00	0.00000E+00	0.00000E+00	0.00000E+00
0.2	-3.66433E-03	1.79912E-02	-4.85078E-03	3.87085E-02
0.4	-7.36743E-03	3.63673E-02	-9.51399E-03	7.60009E-02
0.6	-1.11469E-02	5.55026E-02	-1.38049E-02	1.10486E-01
0.8	-1.50404E-02	7.57705E-02	-1.75389E-02	1.40776E-01
1.0	-1.90849E-02	9.75410E-02	-2.05323E-02	1.65489E-01
1.2	-2.33069E-02	1.21097E-01	-2.26328E-02	1.83491E-01
1.4	-2.77067E-02	1.46522E-01	-2.37700E-02	1.94259E-01
1.6	-3.22783E-02	1.73849E-01	-2.38924E-02	1.97411E-01
1.8	-3.70157E-02	2.03113E-01	-2.29484E-02	1.92568E-01
2.0	-4.19129E-02	2.34349E-01	-2.08866E-02	1.79350E-01
2.2	-4.69593E-02	2.67551E-01	-1.76726E-02	1.57498E-01
2.4	-5.21133E-02	3.02464E-01	-1.33749E-02	1.27535E-01
2.6	-5.73178E-02	3.38699E-01	-8.11306E-03	9.03771E-02
2.8	-6.25148E-02	3.75866E-01	-2.00818E-03	4.69557E-02
3.0	-6.76465E-02	4.13570E-01	4.81810E-03	-1.79323E-03
3.2	-7.26529E-02	4.51394E-01	1.22362E-02	-5.48712E-02
3.4	-7.74733E-02	4.88887E-01	2.00806E-02	-1.11036E-01
3.6	-8.20387E-02	5.25517E-01	2.81537E-02	-1.68785E-01
3.8	-8.62795E-02	5.60747E-01	3.62564E-02	-2.26605E-01
4.0	-9.01262E-02	5.94041E-01	4.41899E-02	-2.82984E-01
4.2	-9.35173E-02	6.24923E-01	5.17686E-02	-3.36533E-01
4.4	-9.64258E-02	6.53160E-01	5.88619E-02	-3.86330E-01
4.6	-9.88299E-02	6.78536E-01	6.53462E-02	-4.31485E-01
4.8	-1.00707E-01	7.00829E-01	7.10972E-02	-4.71101E-01
5.0	-1.02035E-01	7.19815E-01	7.59904E-02	-5.04279E-01
5.2	-1.02797E-01	7.35295E-01	7.99146E-02	-5.30213E-01
5.4	-1.03030E-01	7.47444E-01	8.28767E-02	-5.48971E-01
5.6	-1.02791E-01	7.56549E-01	8.49258E-02	-5.60920E-01
5.8	-1.02138E-01	7.62895E-01	8.61105E-02	-5.66420E-01
6.0	-1.01126E-01	7.66766E-01	8.64794E-02	-5.65831E-01
6.2	-9.98113E-02	7.68452E-01	8.60852E-02	-5.59541E-01
6.4	-9.82589E-02	7.68310E-01	8.50104E-02	-5.48148E-01
6.6	-9.65376E-02	7.66742E-01	8.33503E-02	-5.32350E-01
6.8	-9.47166E-02	7.64157E-01	8.12005E-02	-5.12848E-01
7.0	-9.28654E-02	7.60960E-01	7.86569E-02	-4.90343E-01
7.2	-9.10470E-02	7.57517E-01	7.58075E-02	-4.65474E-01
7.4	-8.93008E-02	7.54050E-01	7.27099E-02	-4.38625E-01
7.6	-8.76647E-02	7.50797E-01	6.94206E-02	-4.10187E-01
7.8	-8.61770E-02	7.48002E-01	6.59968E-02	-3.80560E-01
8.0	-8.48760E-02	7.45906E-01	6.24958E-02	-3.50145E-01
8.2	-8.37954E-02	7.44731E-01	5.89758E-02	-3.19358E-01
8.4	-8.29386E-02	7.44511E-01	5.54553E-02	-2.88322E-01
8.6	-8.23012E-02	7.45243E-01	5.19328E-02	-2.57014E-01
8.8	-8.18792E-02	7.46929E-01	4.84075E-02	-2.25416E-01

Continued

Table A2. Concluded.

α_T (deg)	a_{0,α_T}	a_{1,α_T}	a_{2,α_T}	a_{12,α_T}
9.0	-8.16686E-02	7.49571E-01	4.48788E-02	-1.93514E-01
9.2	-8.16616E-02	7.53145E-01	4.13413E-02	-1.61260E-01
9.4	-8.18320E-02	7.57509E-01	3.77661E-02	-1.28425E-01
9.6	-8.21512E-02	7.62511E-01	3.41208E-02	-9.47648E-02
9.8	-8.25912E-02	7.68004E-01	3.03735E-02	-6.00413E-02
10.0	-8.31237E-02	7.73843E-01	2.64926E-02	-2.40166E-02
10.2	-8.37225E-02	7.79891E-01	2.24518E-02	1.35041E-02
10.4	-8.43710E-02	7.86079E-01	1.82505E-02	5.25017E-02
10.6	-8.50544E-02	7.92342E-01	1.38940E-02	9.29170E-02
10.8	-8.57574E-02	7.98612E-01	9.38673E-03	1.34697E-01
11.0	-8.64647E-02	8.04821E-01	4.73337E-03	1.77788E-01
11.2	-8.71638E-02	8.10917E-01	-5.73920E-05	2.22107E-01
11.4	-8.78547E-02	8.16934E-01	-4.95887E-03	2.67430E-01
11.6	-8.85401E-02	8.22914E-01	-9.94226E-03	3.13521E-01
11.8	-8.92220E-02	8.28896E-01	-1.49794E-02	3.60150E-01
12.0	-8.99025E-02	8.34921E-01	-2.00422E-02	4.07088E-01
12.2	-9.05843E-02	8.41031E-01	-2.51045E-02	4.54120E-01
12.4	-9.12754E-02	8.47299E-01	-3.01439E-02	5.01066E-01
12.6	-9.19842E-02	8.53796E-01	-3.51417E-02	5.47786E-01
12.8	-9.27184E-02	8.60585E-01	-4.00801E-02	5.94147E-01
13.0	-9.34860E-02	8.67731E-01	-4.49410E-02	6.40019E-01
13.2	-9.42945E-02	8.75295E-01	-4.97085E-02	6.85282E-01
13.4	-9.51491E-02	8.83320E-01	-5.43819E-02	7.29938E-01
13.6	-9.60528E-02	8.91833E-01	-5.89690E-02	7.74056E-01
13.8	-9.70089E-02	9.00858E-01	-6.34776E-02	8.17709E-01
14.0	-9.80203E-02	9.10421E-01	-6.79158E-02	8.60969E-01
14.2	-9.90893E-02	9.20540E-01	-7.22935E-02	9.03920E-01
14.4	-1.00214E-01	9.31200E-01	-7.66289E-02	9.46710E-01
14.6	-1.01390E-01	9.42375E-01	-8.09436E-02	9.89505E-01
14.8	-1.02614E-01	9.54037E-01	-8.52589E-02	1.03247E+00
15.0	-1.03883E-01	9.66160E-01	-8.95962E-02	1.07579E+00
15.2	-1.05193E-01	9.78716E-01	-9.39737E-02	1.11958E+00
15.4	-1.06540E-01	9.91665E-01	-9.83973E-02	1.16389E+00
15.6	-1.07918E-01	1.00495E+00	-1.02868E-01	1.20871E+00
15.8	-1.09321E-01	1.01853E+00	-1.07388E-01	1.25403E+00
16.0	-1.10744E-01	1.03233E+00	-1.11959E-01	1.29985E+00
16.2	-1.12182E-01	1.04631E+00	-1.16580E-01	1.34615E+00
16.4	-1.13631E-01	1.06044E+00	-1.21245E-01	1.39286E+00
16.6	-1.15089E-01	1.07466E+00	-1.25943E-01	1.43989E+00
16.8	-1.16552E-01	1.08896E+00	-1.30666E-01	1.48714E+00
17.0	-1.18019E-01	1.10330E+00	-1.35402E-01	1.53452E+00

Table A3. Model for $C_{m,SLCP}$ - SSRS parachute.

α_T (deg)	a_{0,α_T}	a_{1,α_T}	a_{2,α_T}	a_{12,α_T}
0.0	0.00000E+00	0.00000E+00	0.00000E+00	0.00000E+00
0.2	5.98785E-03	-2.98244E-02	7.58273E-03	-6.31669E-02
0.4	1.20349E-02	-6.02444E-02	1.48736E-02	-1.24103E-01
0.6	1.81987E-02	-9.18391E-02	2.15850E-02	-1.80618E-01
0.8	2.45364E-02	-1.25186E-01	2.74299E-02	-2.30524E-01
1.0	3.11048E-02	-1.60858E-01	3.21224E-02	-2.71646E-01
1.2	3.79438E-02	-1.99292E-01	3.54259E-02	-3.02196E-01
1.4	4.50543E-02	-2.40620E-01	3.72300E-02	-3.21337E-01
1.6	5.24276E-02	-2.84904E-01	3.74533E-02	-3.28452E-01
1.8	6.00554E-02	-3.32206E-01	3.60144E-02	-3.22924E-01
2.0	6.79292E-02	-3.82588E-01	3.28318E-02	-3.04134E-01
2.2	7.60333E-02	-4.36052E-01	2.78508E-02	-2.71661E-01
2.4	8.43053E-02	-4.92212E-01	2.11764E-02	-2.26301E-01
2.6	9.26583E-02	-5.50479E-01	1.29932E-02	-1.69472E-01
2.8	1.01005E-01	-6.10260E-01	3.48762E-03	-1.02608E-01
3.0	1.09257E-01	-6.70957E-01	-7.15270E-03	-2.71537E-02
3.2	1.17323E-01	-7.31931E-01	-1.87268E-02	5.53399E-02
3.4	1.25111E-01	-7.92481E-01	-3.09765E-02	1.42920E-01
3.6	1.32513E-01	-8.51785E-01	-4.35936E-02	2.33232E-01
3.8	1.39423E-01	-9.09009E-01	-5.62679E-02	3.23901E-01
4.0	1.45735E-01	-9.63322E-01	-6.86894E-02	4.12556E-01
4.2	1.51352E-01	-1.01398E+00	-8.05688E-02	4.97016E-01
4.4	1.56233E-01	-1.06061E+00	-9.16993E-02	5.75801E-01
4.6	1.60342E-01	-1.10285E+00	-1.01885E-01	6.47477E-01
4.8	1.63641E-01	-1.14034E+00	-1.10928E-01	7.10598E-01
5.0	1.66095E-01	-1.17271E+00	-1.18631E-01	7.63715E-01
5.2	1.67674E-01	-1.19961E+00	-1.24817E-01	8.05529E-01
5.4	1.68434E-01	-1.22130E+00	-1.29493E-01	8.36101E-01
5.6	1.68459E-01	-1.23818E+00	-1.32729E-01	8.55944E-01
5.8	1.67830E-01	-1.25065E+00	-1.34595E-01	8.65562E-01
6.0	1.66630E-01	-1.25910E+00	-1.35161E-01	8.65456E-01
6.2	1.64943E-01	-1.26395E+00	-1.34503E-01	8.56176E-01
6.4	1.62863E-01	-1.26572E+00	-1.32745E-01	8.38617E-01
6.6	1.60495E-01	-1.26502E+00	-1.30033E-01	8.13840E-01
6.8	1.57943E-01	-1.26245E+00	-1.26514E-01	7.82912E-01
7.0	1.55312E-01	-1.25862E+00	-1.22333E-01	7.46900E-01
7.2	1.52696E-01	-1.25409E+00	-1.17626E-01	7.06777E-01
7.4	1.50158E-01	-1.24920E+00	-1.12484E-01	6.63153E-01
7.6	1.47757E-01	-1.24434E+00	-1.06998E-01	6.16665E-01
7.8	1.45553E-01	-1.23990E+00	-1.01261E-01	5.67966E-01
8.0	1.43609E-01	-1.23628E+00	-9.53658E-02	5.17712E-01
8.2	1.41978E-01	-1.23384E+00	-8.94064E-02	4.66580E-01
8.4	1.40669E-01	-1.23267E+00	-8.34179E-02	4.14813E-01
8.6	1.39680E-01	-1.23281E+00	-7.74066E-02	3.62445E-01
8.8	1.39012E-01	-1.23432E+00	-7.13795E-02	3.09520E-01

Continued

Table A3. Concluded.

α_T (deg)	a_{0,α_T}	a_{1,α_T}	a_{2,α_T}	a_{12,α_T}
9.0	1.38662E-01	-1.23726E+00	-6.53441E-02	2.56085E-01
9.2	1.38624E-01	-1.24162E+00	-5.93003E-02	2.02135E-01
9.4	1.38863E-01	-1.24723E+00	-5.32109E-02	1.47379E-01
9.6	1.39340E-01	-1.25392E+00	-4.70337E-02	9.15058E-02
9.8	1.40017E-01	-1.26149E+00	-4.07273E-02	3.42105E-02
10.0	1.40855E-01	-1.26978E+00	-3.42505E-02	-2.48093E-02
10.2	1.41819E-01	-1.27860E+00	-2.75690E-02	-8.58021E-02
10.4	1.42884E-01	-1.28787E+00	-2.06837E-02	-1.48722E-01
10.6	1.44027E-01	-1.29748E+00	-1.36019E-02	-2.13487E-01
10.8	1.45225E-01	-1.30733E+00	-6.32954E-03	-2.80023E-01
11.0	1.46453E-01	-1.31729E+00	1.12723E-03	-3.48258E-01
11.2	1.47692E-01	-1.32730E+00	8.75638E-03	-4.18079E-01
11.4	1.48940E-01	-1.33738E+00	1.65199E-02	-4.89165E-01
11.6	1.50200E-01	-1.34757E+00	2.43776E-02	-5.61190E-01
11.8	1.51470E-01	-1.35792E+00	3.22903E-02	-6.33836E-01
12.0	1.52754E-01	-1.36847E+00	4.02190E-02	-7.06788E-01
12.2	1.54052E-01	-1.37925E+00	4.81277E-02	-7.79753E-01
12.4	1.55375E-01	-1.39037E+00	5.59864E-02	-8.52492E-01
12.6	1.56733E-01	-1.40190E+00	6.37705E-02	-9.24826E-01
12.8	1.58136E-01	-1.41394E+00	7.14570E-02	-9.96591E-01
13.0	1.59594E-01	-1.42655E+00	7.90225E-02	-1.06762E+00
13.2	1.61117E-01	-1.43982E+00	8.64468E-02	-1.13778E+00
13.4	1.62712E-01	-1.45380E+00	9.37313E-02	-1.20708E+00
13.6	1.64383E-01	-1.46853E+00	1.00890E-01	-1.27565E+00
13.8	1.66135E-01	-1.48403E+00	1.07938E-01	-1.34363E+00
14.0	1.67971E-01	-1.50036E+00	1.14888E-01	-1.41114E+00
14.2	1.69895E-01	-1.51753E+00	1.21759E-01	-1.47833E+00
14.4	1.71904E-01	-1.53551E+00	1.28578E-01	-1.54543E+00
14.6	1.73992E-01	-1.55428E+00	1.35379E-01	-1.61269E+00
14.8	1.76155E-01	-1.57380E+00	1.42195E-01	-1.68038E+00
15.0	1.78387E-01	-1.59403E+00	1.49057E-01	-1.74876E+00
15.2	1.80684E-01	-1.61493E+00	1.55996E-01	-1.81803E+00
15.4	1.83039E-01	-1.63644E+00	1.63017E-01	-1.88823E+00
15.6	1.85444E-01	-1.65849E+00	1.70121E-01	-1.95934E+00
15.8	1.87890E-01	-1.68098E+00	1.77310E-01	-2.03132E+00
16.0	1.90368E-01	-1.70385E+00	1.84584E-01	-2.10416E+00
16.2	1.92871E-01	-1.72700E+00	1.91942E-01	-2.17781E+00
16.4	1.95392E-01	-1.75038E+00	1.99373E-01	-2.25215E+00
16.6	1.97928E-01	-1.77392E+00	2.06859E-01	-2.32703E+00
16.8	2.00473E-01	-1.79759E+00	2.14383E-01	-2.40227E+00
17.0	2.03024E-01	-1.82132E+00	2.21931E-01	-2.47773E+00

Table A4. Model for C_T - DGB parachute.

α_T (deg)	a_{0,α_T}	a_{1,α_T}	a_{2,α_T}	a_{12,α_T}
0.0	5.63471E-01	-4.81181E-01	1.10486E-01	-5.38117E-01
0.2	5.63647E-01	-4.82110E-01	1.10750E-01	-5.39177E-01
0.4	5.64154E-01	-4.84682E-01	1.11555E-01	-5.42598E-01
0.6	5.64957E-01	-4.88580E-01	1.12916E-01	-5.48701E-01
0.8	5.66023E-01	-4.93486E-01	1.14848E-01	-5.57808E-01
1.0	5.67317E-01	-4.99083E-01	1.17366E-01	-5.70237E-01
1.2	5.68803E-01	-5.05039E-01	1.20489E-01	-5.86360E-01
1.4	5.70440E-01	-5.10975E-01	1.24240E-01	-6.06610E-01
1.6	5.72184E-01	-5.16527E-01	1.28624E-01	-6.31288E-01
1.8	5.73993E-01	-5.21333E-01	1.33650E-01	-6.60689E-01
2.0	5.75827E-01	-5.25034E-01	1.39321E-01	-6.95105E-01
2.2	5.77646E-01	-5.27300E-01	1.45638E-01	-7.34754E-01
2.4	5.79420E-01	-5.27946E-01	1.52571E-01	-7.79551E-01
2.6	5.81123E-01	-5.26817E-01	1.60082E-01	-8.29342E-01
2.8	5.82728E-01	-5.23757E-01	1.68135E-01	-8.83969E-01
3.0	5.84208E-01	-5.18613E-01	1.76695E-01	-9.43276E-01
3.2	5.85539E-01	-5.11275E-01	1.85717E-01	-1.00702E+00
3.4	5.86719E-01	-5.01865E-01	1.95120E-01	-1.07455E+00
3.6	5.87750E-01	-4.90574E-01	2.04811E-01	-1.14505E+00
3.8	5.88635E-01	-4.77598E-01	2.14699E-01	-1.21773E+00
4.0	5.89376E-01	-4.63130E-01	2.24690E-01	-1.29179E+00
4.2	5.89979E-01	-4.47401E-01	2.34687E-01	-1.36639E+00
4.4	5.90467E-01	-4.30793E-01	2.44575E-01	-1.44042E+00
4.6	5.90863E-01	-4.13737E-01	2.54230E-01	-1.51274E+00
4.8	5.91194E-01	-3.96660E-01	2.63532E-01	-1.58218E+00
5.0	5.91484E-01	-3.79992E-01	2.72358E-01	-1.64758E+00
5.2	5.91766E-01	-3.64191E-01	2.80582E-01	-1.70774E+00
5.4	5.92069E-01	-3.49665E-01	2.88110E-01	-1.76176E+00
5.6	5.92422E-01	-3.36746E-01	2.94876E-01	-1.80898E+00
5.8	5.92849E-01	-3.25769E-01	3.00816E-01	-1.84876E+00
6.0	5.93378E-01	-3.17066E-01	3.05862E-01	-1.88046E+00
6.2	5.94032E-01	-3.10934E-01	3.09960E-01	-1.90353E+00
6.4	5.94824E-01	-3.07485E-01	3.13105E-01	-1.91795E+00
6.6	5.95758E-01	-3.06769E-01	3.15312E-01	-1.92388E+00
6.8	5.96842E-01	-3.08837E-01	3.16597E-01	-1.92147E+00
7.0	5.98081E-01	-3.13739E-01	3.16974E-01	-1.91088E+00
7.2	5.99482E-01	-3.21495E-01	3.16463E-01	-1.89233E+00
7.4	6.01031E-01	-3.31930E-01	3.15145E-01	-1.86662E+00
7.6	6.02713E-01	-3.44778E-01	3.13124E-01	-1.83480E+00
7.8	6.04507E-01	-3.59775E-01	3.10509E-01	-1.79793E+00
8.0	6.06396E-01	-3.76658E-01	3.07405E-01	-1.75707E+00
8.2	6.08361E-01	-3.95150E-01	3.03924E-01	-1.71332E+00
8.4	6.10375E-01	-4.14888E-01	3.00208E-01	-1.66803E+00
8.6	6.12409E-01	-4.35473E-01	2.96411E-01	-1.62273E+00
8.8	6.14433E-01	-4.56504E-01	2.92690E-01	-1.57892E+00

Continued

Table A4. Concluded.

α_T (deg)	a_{0,α_T}	a_{1,α_T}	a_{2,α_T}	a_{12,α_T}
9.0	6.16417E-01	-4.77582E-01	2.89201E-01	-1.53810E+00
9.2	6.18333E-01	-4.98321E-01	2.86097E-01	-1.50174E+00
9.4	6.20157E-01	-5.18406E-01	2.83513E-01	-1.47111E+00
9.6	6.21869E-01	-5.37540E-01	2.81578E-01	-1.44741E+00
9.8	6.23445E-01	-5.55427E-01	2.80423E-01	-1.43186E+00
10.0	6.24865E-01	-5.71771E-01	2.80179E-01	-1.42566E+00
10.2	6.26112E-01	-5.86341E-01	2.80950E-01	-1.42979E+00
10.4	6.27196E-01	-5.99212E-01	2.82730E-01	-1.44409E+00
10.6	6.28135E-01	-6.10540E-01	2.85472E-01	-1.46807E+00
10.8	6.28946E-01	-6.20485E-01	2.89133E-01	-1.50122E+00
11.0	6.29646E-01	-6.29204E-01	2.93666E-01	-1.54304E+00
11.2	6.30252E-01	-6.36863E-01	2.99021E-01	-1.59297E+00
11.4	6.30791E-01	-6.43721E-01	3.05086E-01	-1.64992E+00
11.6	6.31295E-01	-6.50093E-01	3.11723E-01	-1.71253E+00
11.8	6.31795E-01	-6.56288E-01	3.18791E-01	-1.77943E+00
12.0	6.32323E-01	-6.62621E-01	3.26150E-01	-1.84927E+00
12.2	6.32912E-01	-6.69409E-01	3.33651E-01	-1.92061E+00
12.4	6.33593E-01	-6.76954E-01	3.41119E-01	-1.99182E+00
12.6	6.34397E-01	-6.85546E-01	3.48371E-01	-2.06120E+00
12.8	6.35355E-01	-6.95474E-01	3.55223E-01	-2.12708E+00
13.0	6.36497E-01	-7.07029E-01	3.61495E-01	-2.18776E+00
13.2	6.37853E-01	-7.20478E-01	3.67009E-01	-2.24163E+00
13.4	6.39441E-01	-7.35980E-01	3.71615E-01	-2.28736E+00
13.6	6.41275E-01	-7.53652E-01	3.75178E-01	-2.32373E+00
13.8	6.43371E-01	-7.73614E-01	3.77558E-01	-2.34953E+00
14.0	6.45743E-01	-7.95984E-01	3.78618E-01	-2.36354E+00
14.2	6.48403E-01	-8.20863E-01	3.78231E-01	-2.36464E+00
14.4	6.51354E-01	-8.48236E-01	3.76337E-01	-2.35234E+00
14.6	6.54588E-01	-8.78040E-01	3.72905E-01	-2.32640E+00
14.8	6.58102E-01	-9.10210E-01	3.67902E-01	-2.28655E+00
15.0	6.61891E-01	-9.44683E-01	3.61297E-01	-2.23256E+00
15.2	6.65948E-01	-9.81378E-01	3.53077E-01	-2.16435E+00
15.4	6.70249E-01	-1.02010E+00	3.43357E-01	-2.08293E+00
15.6	6.74767E-01	-1.06061E+00	3.32298E-01	-1.98974E+00
15.8	6.79471E-01	-1.10265E+00	3.20064E-01	-1.88625E+00
16.0	6.84334E-01	-1.14598E+00	3.06820E-01	-1.77388E+00
16.2	6.89328E-01	-1.19036E+00	2.92729E-01	-1.65411E+00
16.4	6.94425E-01	-1.23558E+00	2.77953E-01	-1.52834E+00
16.6	6.99602E-01	-1.28145E+00	2.62658E-01	-1.39804E+00
16.8	7.04833E-01	-1.32775E+00	2.47009E-01	-1.26462E+00
17.0	7.10094E-01	-1.37429E+00	2.31168E-01	-1.12953E+00

Table A5. Model for C_N - DGB parachute.

α_T (deg)	a_{0,α_T}	a_{1,α_T}	a_{2,α_T}	a_{12,α_T}
0.0	0.00000E+00	0.00000E+00	0.00000E+00	0.00000E+00
0.2	-3.21254E-03	2.40254E-02	-4.45051E-03	3.66812E-02
0.4	-6.36652E-03	4.75859E-02	-8.94423E-03	7.38380E-02
0.6	-9.40375E-03	7.02197E-02	-1.35239E-02	1.11941E-01
0.8	-1.22660E-02	9.14650E-02	-1.82321E-02	1.51462E-01
1.0	-1.48951E-02	1.10860E-01	-2.31117E-02	1.92870E-01
1.2	-1.72391E-02	1.28002E-01	-2.81926E-02	2.36510E-01
1.4	-1.92747E-02	1.42745E-01	-3.34553E-02	2.82242E-01
1.6	-2.09874E-02	1.55023E-01	-3.88688E-02	3.29824E-01
1.8	-2.23629E-02	1.64767E-01	-4.44030E-02	3.79018E-01
2.0	-2.33867E-02	1.71910E-01	-5.00275E-02	4.29587E-01
2.2	-2.40527E-02	1.76459E-01	-5.57009E-02	4.81178E-01
2.4	-2.43879E-02	1.78707E-01	-6.13372E-02	5.32993E-01
2.6	-2.44281E-02	1.79024E-01	-6.68375E-02	5.84112E-01
2.8	-2.42093E-02	1.77781E-01	-7.21030E-02	6.33613E-01
3.0	-2.37673E-02	1.75350E-01	-7.70348E-02	6.80576E-01
3.2	-2.31419E-02	1.72128E-01	-8.15358E-02	7.24090E-01
3.4	-2.23834E-02	1.68584E-01	-8.55221E-02	7.63346E-01
3.6	-2.15442E-02	1.65194E-01	-8.89131E-02	7.97554E-01
3.8	-2.06769E-02	1.62437E-01	-9.16283E-02	8.25928E-01
4.0	-1.98338E-02	1.60791E-01	-9.35872E-02	8.47679E-01
4.2	-1.90651E-02	1.60702E-01	-9.47225E-02	8.62148E-01
4.4	-1.84036E-02	1.62425E-01	-9.50356E-02	8.69304E-01
4.6	-1.78767E-02	1.66154E-01	-9.45479E-02	8.69297E-01
4.8	-1.75117E-02	1.72082E-01	-9.32810E-02	8.62280E-01
5.0	-1.73357E-02	1.80404E-01	-9.12563E-02	8.48404E-01
5.2	-1.73673E-02	1.91221E-01	-8.85179E-02	8.28033E-01
5.4	-1.75805E-02	2.04187E-01	-8.52207E-02	8.02590E-01
5.6	-1.79344E-02	2.18803E-01	-8.15597E-02	7.73877E-01
5.8	-1.83879E-02	2.34567E-01	-7.77303E-02	7.43696E-01
6.0	-1.89000E-02	2.50979E-01	-7.39274E-02	7.13853E-01
6.2	-1.94291E-02	2.67539E-01	-7.03422E-02	6.86114E-01
6.4	-1.99328E-02	2.83740E-01	-6.71441E-02	6.62067E-01
6.6	-2.03685E-02	2.99079E-01	-6.44958E-02	6.43247E-01
6.8	-2.06937E-02	3.13051E-01	-6.25600E-02	6.31185E-01
7.0	-2.08660E-02	3.25152E-01	-6.14993E-02	6.27413E-01
7.2	-2.08461E-02	3.34918E-01	-6.14628E-02	6.33339E-01
7.4	-2.06197E-02	3.42145E-01	-6.25021E-02	6.49468E-01
7.6	-2.01830E-02	3.46738E-01	-6.46259E-02	6.75920E-01
7.8	-1.95325E-02	3.48602E-01	-6.78430E-02	7.12812E-01
8.0	-1.86645E-02	3.47644E-01	-7.21618E-02	7.60261E-01
8.2	-1.75806E-02	3.43825E-01	-7.75739E-02	8.18225E-01
8.4	-1.63114E-02	3.37422E-01	-8.39684E-02	8.85696E-01
8.6	-1.48997E-02	3.28835E-01	-9.11895E-02	9.61247E-01
8.8	-1.33885E-02	3.18466E-01	-9.90811E-02	1.04345E+00

Continued

Table A5. Concluded.

α_T (deg)	a_{0,α_T}	a_{1,α_T}	a_{2,α_T}	a_{12,α_T}
9.0	-1.18208E-02	3.06716E-01	-1.07487E-01	1.13088E+00
9.2	-1.02412E-02	2.94010E-01	-1.16246E-01	1.22206E+00
9.4	-8.70518E-03	2.80902E-01	-1.25160E-01	1.31513E+00
9.6	-7.27204E-03	2.67998E-01	-1.34012E-01	1.40807E+00
9.8	-6.00116E-03	2.55900E-01	-1.42587E-01	1.49888E+00
10.0	-4.95189E-03	2.45211E-01	-1.50671E-01	1.58554E+00
10.2	-4.17627E-03	2.36475E-01	-1.58068E-01	1.66621E+00
10.4	-3.69988E-03	2.30011E-01	-1.64671E-01	1.73984E+00
10.6	-3.53934E-03	2.26060E-01	-1.70399E-01	1.80559E+00
10.8	-3.71109E-03	2.24861E-01	-1.75171E-01	1.86266E+00
11.0	-4.23158E-03	2.26655E-01	-1.78907E-01	1.91024E+00
11.2	-5.11372E-03	2.31647E-01	-1.81538E-01	1.94762E+00
11.4	-6.34811E-03	2.39823E-01	-1.83071E-01	1.97480E+00
11.6	-7.91623E-03	2.51085E-01	-1.83542E-01	1.99207E+00
11.8	-9.79951E-03	2.65331E-01	-1.82991E-01	1.99973E+00
12.0	-1.19794E-02	2.82464E-01	-1.81455E-01	1.99809E+00
12.2	-1.44342E-02	3.02347E-01	-1.78984E-01	1.98756E+00
12.4	-1.71284E-02	3.24698E-01	-1.75682E-01	1.96908E+00
12.6	-2.00228E-02	3.49190E-01	-1.71663E-01	1.94370E+00
12.8	-2.30778E-02	3.75495E-01	-1.67045E-01	1.91252E+00
13.0	-2.62542E-02	4.03286E-01	-1.61944E-01	1.87659E+00
13.2	-2.95149E-02	4.32255E-01	-1.56472E-01	1.83695E+00
13.4	-3.28285E-02	4.62127E-01	-1.50733E-01	1.79459E+00
13.6	-3.61637E-02	4.92624E-01	-1.44834E-01	1.75050E+00
13.8	-3.94893E-02	5.23466E-01	-1.38883E-01	1.70570E+00
14.0	-4.27740E-02	5.54373E-01	-1.32985E-01	1.66121E+00
14.2	-4.59888E-02	5.85084E-01	-1.27241E-01	1.61796E+00
14.4	-4.91157E-02	6.15420E-01	-1.21719E-01	1.57661E+00
14.6	-5.21403E-02	6.45229E-01	-1.16474E-01	1.53773E+00
14.8	-5.50482E-02	6.74361E-01	-1.11564E-01	1.50187E+00
15.0	-5.78252E-02	7.02666E-01	-1.07044E-01	1.46958E+00
15.2	-6.04596E-02	7.30016E-01	-1.02961E-01	1.44133E+00
15.4	-6.29568E-02	7.56427E-01	-9.93002E-02	1.41698E+00
15.6	-6.53309E-02	7.81986E-01	-9.60201E-02	1.39616E+00
15.8	-6.75958E-02	8.06783E-01	-9.30800E-02	1.37851E+00
16.0	-6.97656E-02	8.30907E-01	-9.04386E-02	1.36365E+00
16.2	-7.18546E-02	8.54450E-01	-8.80540E-02	1.35119E+00
16.4	-7.38776E-02	8.77516E-01	-8.58784E-02	1.34069E+00
16.6	-7.58502E-02	9.00217E-01	-8.38618E-02	1.33169E+00
16.8	-7.77880E-02	9.22662E-01	-8.19542E-02	1.32370E+00
17.0	-7.97062E-02	9.44963E-01	-8.01056E-02	1.31627E+00

Table A6. Model for $C_{m,SLCP}$ - DGB parachute.

α_T (deg)	a_{0,α_T}	a_{1,α_T}	a_{2,α_T}	a_{12,α_T}
0.0	0.00000E+00	0.00000E+00	0.00000E+00	0.00000E+00
0.2	5.56435E-03	-4.20859E-02	7.68344E-03	-6.66235E-02
0.4	1.10322E-02	-8.34040E-02	1.54353E-02	-1.33964E-01
0.6	1.63076E-02	-1.23192E-01	2.33229E-02	-2.02728E-01
0.8	2.12946E-02	-1.60689E-01	3.14137E-02	-2.73622E-01
1.0	2.58974E-02	-1.95132E-01	3.97749E-02	-3.47353E-01
1.2	3.00304E-02	-2.25854E-01	4.84542E-02	-4.24431E-01
1.4	3.36543E-02	-2.52607E-01	5.74181E-02	-5.04596E-01
1.6	3.67451E-02	-2.75273E-01	6.66139E-02	-5.87410E-01
1.8	3.92790E-02	-2.93737E-01	7.59891E-02	-6.72439E-01
2.0	4.12318E-02	-3.07881E-01	8.54916E-02	-7.59250E-01
2.2	4.25932E-02	-3.17707E-01	9.50510E-02	-8.47230E-01
2.4	4.34069E-02	-3.23688E-01	1.04525E-01	-9.35066E-01
2.6	4.37313E-02	-3.26421E-01	1.13750E-01	-1.02125E+00
2.8	4.36249E-02	-3.26505E-01	1.22564E-01	-1.10427E+00
3.0	4.31461E-02	-3.24538E-01	1.30803E-01	-1.18262E+00
3.2	4.23595E-02	-3.21164E-01	1.38308E-01	-1.25483E+00
3.4	4.13469E-02	-3.17134E-01	1.44941E-01	-1.31958E+00
3.6	4.01935E-02	-3.13220E-01	1.50574E-01	-1.37566E+00
3.8	3.89847E-02	-3.10191E-01	1.55076E-01	-1.42181E+00
4.0	3.78058E-02	-3.08819E-01	1.58318E-01	-1.45679E+00
4.2	3.67380E-02	-3.09821E-01	1.60190E-01	-1.47958E+00
4.4	3.58344E-02	-3.13603E-01	1.60700E-01	-1.49020E+00
4.6	3.51389E-02	-3.20472E-01	1.59888E-01	-1.48897E+00
4.8	3.46954E-02	-3.30734E-01	1.57793E-01	-1.47620E+00
5.0	3.45478E-02	-3.44694E-01	1.54455E-01	-1.45224E+00
5.2	3.47256E-02	-3.62513E-01	1.49950E-01	-1.41773E+00
5.4	3.51867E-02	-3.83629E-01	1.44536E-01	-1.37505E+00
5.6	3.58641E-02	-4.07235E-01	1.38537E-01	-1.32719E+00
5.8	3.66911E-02	-4.32519E-01	1.32275E-01	-1.27715E+00
6.0	3.76005E-02	-4.58674E-01	1.26075E-01	-1.22792E+00
6.2	3.85250E-02	-4.84888E-01	1.20252E-01	-1.18242E+00
6.4	3.93962E-02	-5.10358E-01	1.15085E-01	-1.14325E+00
6.6	4.01460E-02	-5.34284E-01	1.10841E-01	-1.11292E+00
6.8	4.07063E-02	-5.55864E-01	1.07785E-01	-1.09391E+00
7.0	4.10088E-02	-5.74300E-01	1.06185E-01	-1.08873E+00
7.2	4.09913E-02	-5.88856E-01	1.06283E-01	-1.09967E+00
7.4	4.06318E-02	-5.99229E-01	1.08162E-01	-1.12750E+00
7.6	3.99267E-02	-6.05293E-01	1.11831E-01	-1.17237E+00
7.8	3.88721E-02	-6.06926E-01	1.17301E-01	-1.23443E+00
8.0	3.74644E-02	-6.04004E-01	1.24582E-01	-1.31380E+00
8.2	3.57079E-02	-5.96495E-01	1.33656E-01	-1.41038E+00
8.4	3.36542E-02	-5.84867E-01	1.44337E-01	-1.52246E+00
8.6	3.13746E-02	-5.69793E-01	1.56367E-01	-1.64768E+00
8.8	2.89407E-02	-5.51947E-01	1.69486E-01	-1.78364E+00

Continued

Table A6. Concluded.

α_T (deg)	a_{0,α_T}	a_{1,α_T}	a_{2,α_T}	a_{12,α_T}
9.0	2.64241E-02	-5.32004E-01	1.83434E-01	-1.92797E+00
9.2	2.38991E-02	-5.10672E-01	1.97944E-01	-2.07821E+00
9.4	2.14559E-02	-4.88854E-01	2.12688E-01	-2.23132E+00
9.6	1.91910E-02	-4.67529E-01	2.27314E-01	-2.38401E+00
9.8	1.72009E-02	-4.47675E-01	2.41470E-01	-2.53299E+00
10.0	1.55820E-02	-4.30270E-01	2.54802E-01	-2.67497E+00
10.2	1.44185E-02	-4.16187E-01	2.66995E-01	-2.80697E+00
10.4	1.37494E-02	-4.05915E-01	2.77876E-01	-2.92732E+00
10.6	1.35990E-02	-3.99808E-01	2.87320E-01	-3.03474E+00
10.8	1.39914E-02	-3.98220E-01	2.95203E-01	-3.12801E+00
11.0	1.49503E-02	-4.01504E-01	3.01400E-01	-3.20586E+00
11.2	1.64944E-02	-4.09960E-01	3.05804E-01	-3.26723E+00
11.4	1.86064E-02	-4.23542E-01	3.08432E-01	-3.31216E+00
11.6	2.12546E-02	-4.42067E-01	3.09348E-01	-3.34120E+00
11.8	2.44071E-02	-4.65348E-01	3.08621E-01	-3.35488E+00
12.0	2.80320E-02	-4.93200E-01	3.06316E-01	-3.35374E+00
12.2	3.20928E-02	-5.25387E-01	3.02520E-01	-3.33851E+00
12.4	3.65324E-02	-5.61454E-01	2.97400E-01	-3.31069E+00
12.6	4.12881E-02	-6.00881E-01	2.91142E-01	-3.27203E+00
12.8	4.62969E-02	-6.43148E-01	2.83937E-01	-3.22423E+00
13.0	5.14962E-02	-6.87736E-01	2.75970E-01	-3.16903E+00
13.2	5.68269E-02	-7.34157E-01	2.67424E-01	-3.10808E+00
13.4	6.22401E-02	-7.81990E-01	2.58464E-01	-3.04293E+00
13.6	6.76877E-02	-8.30811E-01	2.49258E-01	-2.97517E+00
13.8	7.31214E-02	-8.80196E-01	2.39976E-01	-2.90637E+00
14.0	7.84929E-02	-9.29720E-01	2.30785E-01	-2.83812E+00
14.2	8.37577E-02	-9.78987E-01	2.21842E-01	-2.77189E+00
14.4	8.88889E-02	-1.02773E+00	2.13253E-01	-2.70869E+00
14.6	9.38654E-02	-1.07575E+00	2.05102E-01	-2.64936E+00
14.8	9.86666E-02	-1.12281E+00	1.97476E-01	-2.59473E+00
15.0	1.03272E-01	-1.16870E+00	1.90459E-01	-2.54565E+00
15.2	1.07663E-01	-1.21325E+00	1.84123E-01	-2.50281E+00
15.4	1.11850E-01	-1.25646E+00	1.78443E-01	-2.46599E+00
15.6	1.15853E-01	-1.29846E+00	1.73356E-01	-2.43462E+00
15.8	1.19694E-01	-1.33940E+00	1.68795E-01	-2.40812E+00
16.0	1.23393E-01	-1.37938E+00	1.64696E-01	-2.38589E+00
16.2	1.26973E-01	-1.41855E+00	1.60993E-01	-2.36734E+00
16.4	1.30455E-01	-1.45705E+00	1.57613E-01	-2.35179E+00
16.6	1.33863E-01	-1.49504E+00	1.54477E-01	-2.33852E+00
16.8	1.37218E-01	-1.53267E+00	1.51510E-01	-2.32682E+00
17.0	1.40545E-01	-1.57009E+00	1.48634E-01	-2.31596E+00

Acknowledgments

The authors thank the following individuals for their assistance with the work presented herein. Carlie H. Zumwalt, Clara O'Farrell, and Donald F. Keller for making available the unpublished static coefficients source data. Justin S. Green of the NASA Langley Research Center for his assistance with MATLAB[®] analyses and for providing comments regarding the models. Dr. Drew Landman of Old Dominion University for providing advice on the linear regression models and reviewing the manuscript.

References

¹Cruz, J. R., Way, D. W., Shidner, J. D., Davis, J. L., Powell, R. W., Kipp, D. M., Adams, D. S., Sengupta, A., Witkowski, A., and Kandis, M., "Parachute Models Used in the Mars Science Laboratory Entry, Descent, and Landing Simulation, AIAA Paper 2013-1276, presented at the 22nd AIAA Aerodynamic Decelerator Systems Technology Conference and Seminar, Daytona Beach, FL, March 25–28, 2013.

²Zumwalt, C. H., Cruz, J. R., Keller, D. F., and O'Farrell, C., "Wind Tunnel Test of Subscale Ringsail and Disk-Gap-Band Parachutes," AIAA Paper 2016-3426, presented at the 34th AIAA Applied Aerodynamics Conference, Washington, DC, June 13–17, 2016.

³Cruz, J. R., O'Farrell, C., Hennings, E., and Runnells, P., "Permeability of Two Parachute Fabrics – Measurements, Modeling, and Application," NASA TM 2016-219328 (Corrected Copy), July 2016. (Also available as an AIAA paper presented at the 24th AIAA Aerodynamic Decelerator Systems Technology Conference, Denver, CO, June 5-9, 2017.)

⁴Clark, I., Adler, M., Rivellini, T., "Development and Testing of a New Family of Supersonic Decelerators," AIAA Paper 2013-1252, presented at the 22nd AIAA Aerodynamic Decelerator Systems Technology Conference and Seminar, March 25–28, 2013

⁵Parachute Industry Association, "Commercial Specification, Cloth, Parachute, Nylon-Rip Stop and Will Weave," PIA-C-7020D, November 17, 2010.

⁶Parachute Industry Association, "Commercial Specification, Cloth, Parachute, Nylon, Low Permeability," PIA-C-44378D, May 3, 2007.

⁷Lingard, J. and Underwood, J., "The Effect of Low Density Atmospheres on the Aerodynamic Coefficients of Parachutes," AIAA Paper 95-1556, presented at the 13th AIAA Aerodynamic Decelerator Systems Technology Conference, Clearwater, FL, May 15–19, 1995.

⁸Lingard, S., "Aerodynamics 1 (Steady)," lecture notes for the Parachute Systems Technology Short Course, U. S. Army Proving Ground, May 12–16, 2008.

⁹Cruz, J. R. and Snyder, M. L., "Estimates for the Aerodynamic Coefficients of Ringsail and Disk-Gap-Band Parachutes Operating on Mars," NASA Technical Memorandum in preparation, 2017.

¹⁰Cruz, J. R., Way, D. W., Shidner, J. D., Davis, J. L., Adams, D. S., and Kipp, D. M., "Reconstruction of the Mars Science Laboratory Parachute Performance," *Journal of Spacecraft and Rockets*, Vol. 51, No. 4, pp. 1185–1196, July–August 2014.

¹¹Anon., *JMP Statistics and Graphics Guide*, Release 6, SAS Institute Inc., Cary, NC, 2005.